Contrib Mineral Petrol (1985) 90:142–161

Contributions to Mineralogy and Petrology

Jorullo Volcano, Michoacán, Mexico (1759–1774): The earliest stages of fractionation in calc-alkaline magmas

James F. Luhr[1] **and Ian S.E. Carmichael**[2]

[1] Department of Geology, Franklin and Marshall College, Lancaster, PA 17604
[2] Department of Geology and Geophysics, University of California, Berkeley, CA 94720

Abstract. Between 1759 and 1774, Jorullo Volcano and four associated cinder cones erupted an estimated 2 km^3 of magma which evolved progressively with time from early, hypersthene-normative, primitive basalts to late-stage, quartz-normative, basaltic andesites. All lavas contain <6 vol% phenocrysts of magnesian olivine (Fo_{90-70}) with Cr–Al–Mg-spinel inclusions, and microphenocrysts of plagioclase and augite; late-stage basaltic andesites also carry phenocrysts of plagioclase, augite, and rare orthopyroxene, hornblende pseudomorphs, and microphenocrysts of titanomagnetite. Olivine-melt compositions indicate liquidus temperatures ranging from 1,230° C to 1,070° C in the early- and late-stage lavas, respectively; f_{O_2} was about 0.6 log units above the Ni–NiO buffer in the early lavas but increased to 2.5 log units above Ni–NiO in the late lavas, perhaps through groundwater-magma interaction.

Smooth major and trace element compositional trends in the lavas can be largely modeled by simple crystal fractionation of olivine, augite, plagioclase, and minor spinel. La, Ce, and other incompatible elements (Rb, Sr, Ba, Hf, Th, Ta), however, are anomalously enriched in the late-stage lavas, whereas the heavy rare earth elements (Dy, Yb, Lu) are anomalously depleted. The modeled crystal fractionation event must have occurred at lower-crustal to upper-mantle pressures (8–15 kb), although the crystals actually present in the Jorullo lavas appear to have formed at low pressures. Thus, a two-stage crystallization history is implied. Despite the presence of granitic xenoliths in middle-stage lavas from Jorullo, bulk crustal assimilation appears to have played an insignificant role in generating the compositional trends among the lavas.

As MgO decreases from 9.3 to 4.3 wt% through the suite, Al_2O_3 increases from 16.4 to 19.1 wt%. Most high-alumina basalts reported in the literature have 18 to 21 wt% Al_2O_3, but are too depleted in MgO, Ni, and Cr to have been generated directly through mantle partial melting. These high-alumina basalts have probably undergone significant fractionation of olivine, augite, plagioclase, and spinel from primitive parental basalts similar to the early Jorullo lavas. Such primitive basalts are rarely erupted in mature arcs and may be completely absent from mature stratovolcanoes.

Cerro La Pilita is a late-Quaternary cinder and lava cone centered just 3 km south of Jorullo. The primitive trachybasalts of Cerro La Pilita, however, are radically different from the Jorullo basalts. They are nepheline normative with high concentrations of K_2O (>2.5 wt%), P_2O_5 (>0.9 wt%), Ba (1,200 ppm), Sr (>2,000 ppm), and many other incompatible elements, and contain crystals of hornblende and apatite in addition to olivine, spinel, augite, and plagioclase. The magmas of these two neighboring volcanoes cannot be related to one another by any simple mechanism, and must represent fundamentally different partial melting events in the mantle. The contrasts between Jorullo and Cerro La Pilita demonstrate the difficulty in defining simple relationships between magma type and distance from the trench in the Mexican Volcanic Belt.

Offprint requests to: J.F. Luhr

Introduction

The Michoacán-Guanajuato Volcanic Field, located in the western portion of the Mexican Volcanic Belt (Fig. 1), contains one of the greatest concentrations of Quaternary cinder and lava cones on earth (Hasenaka and Carmichael 1985). Of the nearly 1,000 morphologically youthful cones in an area 250 km EW by 200 km NS, two have erupted since the Spanish Conquest: Jorullo (1759–1774) and Parícutin (1943–1952). The birth of Parícutin "in a cornfield" in February 1943 captured the attention of geologists from around the world, and its eruptive history was carefully recorded (Foshag and Gonzalez 1954). The petrologic studies of Wilcox (1954) established a systematic evolution of magmatic compositions with time from early basaltic andesites (55% SiO_2) to later andesites (60% SiO_2). In marked contrast to Parícutin, Jorullo Volcano and its 1759 birth in a narrow ravine have been little studied. The lavas of Jorullo also became more silicic with time, evolving from early, primitive, olivine- and hypersthene-normative basalts (52% SiO_2) to later quartz-normative basaltic andesites (55% SiO_2). Jorullo is one of the southernmost cinder cones in the volcanic field, sitting 75 km southeast of Parícutin, and 240 km northeast of the Middle America Trench, where the Cocos Plate is subducting at an angle of about 30° northeastward beneath the North American Plate. A poorly defined Benioff Zone underlies the Jorullo area at a depth of some 120 km (Molnar and Sykes 1969; Nixon 1982). General treatments of the Michoacán-Guanajuato Volcanic Field can be found in Williams (1950), Demant (1981), and Hasenaka and Carmichael (1985).

In this paper we discuss the 1759–1774 eruption of Jorullo and its satellite cones, documenting the evolution of mineral and lava compositions with time, and presenting a model for these variations. We also discuss data for Cerro

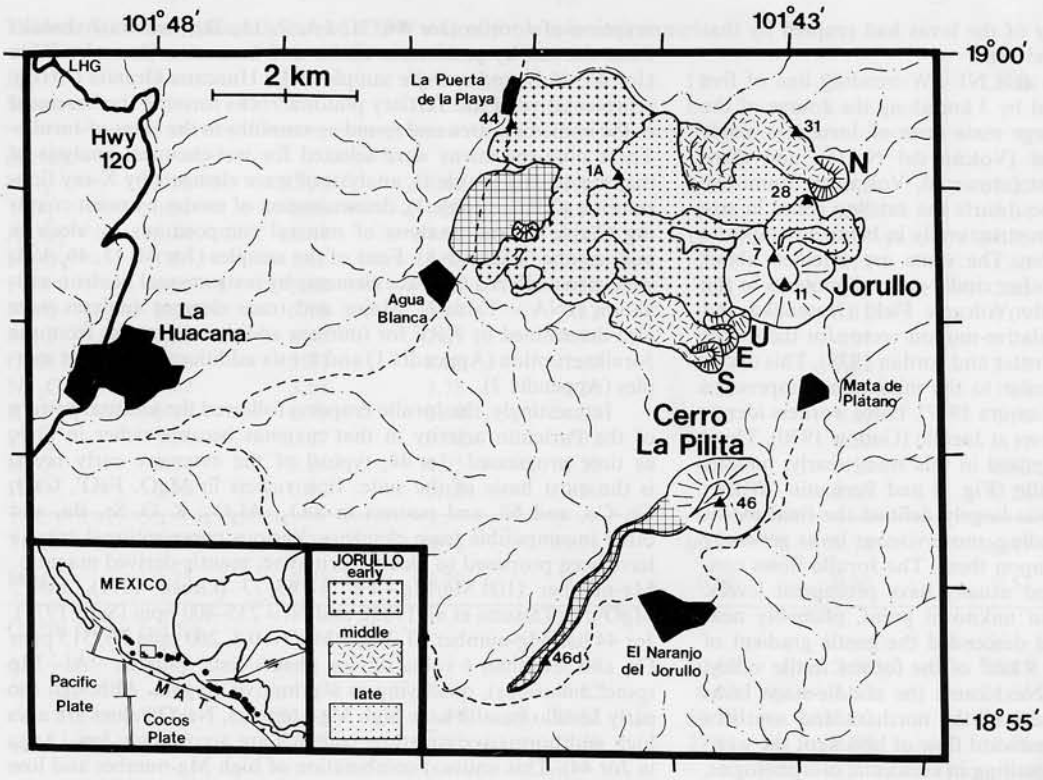

Fig. 1. Location map showing Jorullo Volcano, its four parasitic cones (N = Volcán del Norte, U = unnamed, E = Volcán Enmedio, S = Volcán del Sur), and the three stages of lava flows (see pattern key). Triangles show sample locations and numbers. LHG indicates the sample locality for La Huacana Granite. Cross-hatched pattern shows pre-historic lava flows including that from Cerro La Pilita. Cities and villages are shown in black. Dashed lines are unpaved roads. Dot-dash lines show drainages. On inset map, small square outlines the Michoacán-Guanajuato Volcanic Field, stars show Parícutin and Jorullo, dots represent major composite volcanoes, and MAT = Middle America Trench

La Pilita, an older eruptive center 3 km south of Jorullo's main cone. Trachybasaltic scoria and lava samples from this cone contrast sharply with basalts of neighboring Jorullo in containing high concentrations of K_2O, P_2O_5, Sr, Ba, and other incompatible elements as well as crystals of hornblende and apatite.

The eruption of Jorullo: 1759–1774

The story of the Jorullo eruption was in a state of great confusion for many years, confusion stemming partly from the delayed publication of an eye-witness report to the Spanish Viceroy concerning the early activity, and partly from the erroneous observations of Alexander von Humboldt (1810), who visited the area in 1803. Von Humboldt interpreted the Jorullo lava field as a large volcanic blister which rose from the ground, and his observations inspired the 'craters of elevation' theory of his friend von Buch (Greene 1982). Gadow (1930) gives an insightful account of the eruption and English translations of all important prior observations as a preface to his study of floral and faunal reclamation of the devastated area. Subsequent discussions of the Jorullo eruption (Segerstrom 1950; Mooser 1958; Bullard 1976) including that which follows, have relied heavily on the synthesis of Gadow (1930).

Prior to 1759, the area was a cultivated, west-sloping basin bounded by steeply dissected escarpments of Cenozoic intrusives, tuffs, and lavas. The area has a tropical climate and a general elevation of 600 to 800 m. Famous for its fertility, the land was known as Jorullo, or Paradise, in the Tarascan Indian language. Hacienda de Jorullo was situated near Cerro Partido, which rose as an EW-trending ridge near the basin center (Fig. 1). At the eastern end of the basin was the narrow and deep ravine of the Cuitinga Creek, which followed a NE to SW course before turning west along the granite ridge forming the southern boundary of the basin.

Subterranean noises were first heard in late June of 1759, increasing to the level of cannon shots by September 17. Earthquakes badly damaged structures on the Hacienda. On the morning of September 29, several sharp tremors were felt, and a dense dark cloud issued from the Cuitinga Creek just SE of the Hacienda. The early part of the eruption was characterized by phreatic and phreatomagmatic activity, which blanketed the surrounding area with a sticky mud. Gadow (1930) noted that despite a near absence of precipitation in the fall of 1759, large quantities of water and mud were flowing from the Jorullo area. Numerous springs became active in the surrounding hills and streams alternated between swollen and dry. The eye-witness Sayago described pulses of hot muddy water pouring from small short-lived vents. Ash falls covered the surrounding area and by October 6 the town of La Huacana, 9 km to the west (Fig. 1), was abandoned. Streams choked with ash flooded much of the valley to the west of the volcano, from La Puerta de La Playa to La Huacana. The copious outflow of water in the early stages of the eruption probably resulted from the outward migration of groundwater ahead of the rising magma body as suggested for the 1902 eruption of Mt. Pelee (Robool and Smith 1975; Fisher and Heiken 1982). The first incandescent bombs were noted on October 8, and by October 14, phreatic aspects of the eruption declined in significance as it became dominantly magmatic in character. Water and mud were no longer reported as issuing from the ground. The second and final report of Sayago was written on November 13, by which time the main cone of Jorullo had reached 250 m in height. No lavas had emerged by this date, after which there is unfortunately little reliable reporting. Oral traditions refer to violent eruptions through 1764, the year of greatest activity, and lesser eruptions until 1774. A report for the new Governor in 1766 describes a scene similar to that of today, and Gadow

(1930) argued that the majority of the lavas had erupted by that date, probably between 1760 and 1766.

Magma and gas issued from a NE-SW-trending line of five cinder and lava cones separated by 3 km along the course of the Cuitinga Creek (Fig. 1): the large main cone of Jorullo, a single breached cone to its northeast (Volcán del Norte), and three breached cones to its southwest (unnamed, Volcán de Enmedio, Volcán del Sur). The main cone dwarfs the satellite cones in size and appears to differ from them structurally in being a composite cone of lavas as well as cinder. The vents are oriented about N35° E, sub-parallel to many other cinder-cone alignments in the southern Michoacán-Guanajuato Volcanic Field (Hasenaka and Carmichael (1985) and to the relative-motion vector for the Cocos and North American Plates (Minster and Jordan 1978). This orientation is presumably perpendicular to the minimum compressive stress direction in the area (Nakamura 1977). Early workers identified four to six different lava flows at Jorullo (Gadow 1930). Three lava stages or groups are recognized in this study: early, middle, and late (Fig. 1). At both Jorullo (Fig. 1) and Parícutin (Wilcox 1954), the most-basic, early lavas largely defined the final extent of ground covered, with succeeding, more-viscous lavas generally forming thicker terraced flows upon them. The Jorullo flows consist primarily of block lava and usually have prominent levees. The early lavas issued from an unknown point, probably near the base of the main cone, and descended the gentle gradient of the basin to the west, covering 9 km^2 of the former fertile valley, an area since called Malpais. Next came the middle-stage lavas which breached the western sides of the northern and southern satellite cones. The downhill, westward flow of lava kept the western sides of these cones open, resulting in crescentic morphologies, similar in form to the Sapichu vent at Parícutin (Wilcox 1954). The late-stage lavas issued from the northern side of the main cone. Pyroclastic activity continued through the extrusion of most late-stage lavas, and all lava flows were covered by ash-fall layers. Following the end of pyroclastic activity, a small lava flow then emerged from the main cone, bringing the Jorullo eruption to a close. This black, youngest lava flow is still relatively unvegetated today and stands in sharp visual contrast to the subdued hues of the slightly older, but ash-covered lavas, where vegetation found an easy foothold. Since the end of the eruption, the crater of the main cone has been collapsing inward along arcuate step faults, increasing both the crater diameter (400 m × 500 m) and its depth (150 m) (Mooser 1958).

One of the most curious features of the Jorullo products is the sequence of ash layers that covers all but the youngest of the lava flows. These fine ashes form a mantling blanked of cm-scale layers which show only occasional cross beds, yet cover irregularities on the lava flow surface with slope angles up to 80°. These air-fall ashes must have been extraordinarily cohesive to be able to stick to surfaces with such steep angles. They probably were very wet when falling and upon impact they were almost instantly baked and moderately lithified by the hot underlying lavas, which still showed thousands of hornitos at the time of von Humboldt's visit in 1803.

The main cone of Jorullo (18.97° N, 101.72° W) rises some 350 m above its surroundings to an elevation of 1,220 m. It has a volume of approximately 0.20 km^3 and the smaller parasitic cones have a combined volume of 0.05 km^3. The lavas have an estimated volume of 0.50 km^3, although this figure is made uncertain by a lack of information on the depth of lava close to the vent. The volume of ash-fall deposits is unknown. By analogy with Parícutin, which produced 0.49 km^3 of magma as lavas and 0.83 km^3 of magma as tephra (Fries 1953), the pyroclastic deposits at Jorullo may have represented up to 1.25 km^3 of magma. The total mass of magma erupted at Jorullo, therefore, was possibly 2 km^3.

Sample descriptions and whole-rock compositions

This study is primarily concerned with nine specimens: six basalts and basaltic andesites from successive stages of the 1759–1774 eruption of Jorullo (Jor 44, 31, 1A, 7, 11, 28), two trachybasalts from the nearby prehistoric cinder and lava cone Cerro La Pilita (Jor 46, 46d), and a single sample of La Huacana Granite (LHG), representative of the Tertiary plutonic rocks forming the basement in the immediate area and found as xenoliths in the lavas of Jorullo. These nine specimens were selected for wet-chemical analysis of major elements (Table 1), analysis of trace elements by X-ray fluorescence (XRF – Table 3), determination of modes by point counting (Table 4), and analysis of mineral compositions by electron microprobe (Tables 5–8). Four of the samples (Jor 44, 11, 46, 46d) were also analyzed for trace elements by instrumental neutron activation (INA – Table 2). Major and trace element analyses were also determined by XRF for fourteen additional samples from the Jorullo eruption (Appendix 1) and for six additional basement samples (Appendix 2).

Interestingly, the Jorullo eruption followed the unusual pattern of the Parícutin activity in that magmas became richer in SiO_2 as time progressed. Jor 44, typical of the extensive early lavas, is the most basic of the suite. It is richest in MgO, FeO^t, CaO, Cr, Co, and Ni, and poorest in SiO_2, Al_2O_3, K_2O, Sr, Ba, and other incompatible trace elements. Various compositional criteria have been proposed to identify primitive, mantle-derived magmas: Mg-number ($100\ Mg/Mg+Fe^{2+}$) = 63–73 (Green 1971), $FeO^T/MgO < 1$ (Tatsumi et al. 1983), and Ni = 235–400 ppm (Sato 1977). Jor 44 has Mg-number 73, $FeO^T/MgO = 0.8$, 260 ppm Ni, 515 ppm Cr, and less than 6 vol% olivine phenocrysts (plus Cr–Al–Mg spinel inclusions), qualifying as a primitive magma. Although the early Jorullo basalts have high Mg-numbers, Na_2O values are also high and normative anorthite contents are accordingly low (An_{48} in Jor 44). This unusual combination of high Mg-number and low An content is consistent with a relatively high-pressure source region. The early Jorullo basalts are also relatively silica-rich (52.1 wt% SiO_2 in Jor 44), and in this respect these primitive basalts recall Japanese sanukitoids (Tatsumi and Ishizaka 1982a and 1982b). Sample Jor 31, from Volcan del Norte, is representative of the middle-stage lavas and is only slightly richer in SiO_2 than Jor 44. Sample Jor 1A is from a small extrusive dome near the SW margin of the late lavas (Fig. 1). The dome has no ash cover and therefore probably extruded while the last lavas were issuing from the main cone. Compositionally and mineralogically, however, Jor 1A is most similar to the middle lavas. This small dome may have formed as a squeeze-up from the underlying middle-stage lavas as they were over-ridden by the late-stage flows. Jor 1A is slightly more SiO_2-rich than Jor 31; it is classified as a middle-stage lava in this study. The three late-stage samples (Jor 7, 11, 28) show continued progressive increases in SiO_2, Al_2O_3, and related elements and decreases in MgO, Cr, and Ni. The progressive compositional evolution from early basalts to late-stage basaltic andesites can be seen on MgO-variation diagrams in Fig. 2, where the early, middle, and late Jorullo samples are distinguished by different symbols. The origin of compositional diversity in the Jorullo suite is discussed in a later section. Fig. 3 is a chondrite-normalized rare earth element (REE) plot showing that late-stage Jorullo lava sample 11 is enriched in light REEs, but depleted in heavy REEs compared to early-stage sample 44, resulting in crossed REE patterns.

Cerro La Pilita is a Quaternary-age cinder cone just 3 km SSW of the main cone of Jorullo (Fig. 1). A tongue of lava flowed 4 km down a stream canyon from the SW foot of La Pilita. The total volume of magma erupted from this cone is estimated at 0.6 km^3. Scoria and lava samples (Jor 46, 46d, respectively) are primitive trachybasalts with Mg-numbers = 80, $FeO^T/MgO = 0.94$–0.91, 220–250 ppm Ni, and 330–340 ppm Cr. The Mg-numbers might have been raised by post-eruptive oxidation of iron, but both samples have identical ferric-ferrous ratios, and we suggest that the Mg-numbers and the ferric-ferrous ratios reflect magmatic conditions. The Cerro La Pilita trachybasalts differ dramatically from the calc-alkaline suite of Jorullo. The trachybasalts are nenormative with four- to ten-fold enrichments over the early Jorullo basalts in K_2O (>2.5 wt%), P_2O_5 (>0.9%), Sr (>2,000 ppm), Ba (1,200 ppm), and related elements. The REE plot of Fig. 3 indi-

Table 1. Wet chemical analyses and CIPW norms for whole-rock samples

Jor	44	31	1A	7	11	28	LHG	46	46d
Stage	E	M	M	L	L	L			
(wt%)									
SiO_2	52.10	52.70	53.42	54.84	54.18	54.65	67.20	49.21	51.72
TiO_2	0.81	0.88	1.00	0.99	0.92	0.95	0.64	1.33	1.22
Al_2O_3	16.44	16.84	17.06	18.34	18.74	19.07	14.05	14.19	15.12
Fe_2O_3	1.56	1.68	1.58	2.76	2.47	3.12	1.40	4.54	4.28
FeO	6.05	5.80	5.84	4.10	4.31	3.68	2.83	3.75	3.47
MnO	0.14	0.13	0.14	0.12	0.11	0.11	0.07	0.12	0.12
MgO	9.29	8.46	7.65	4.96	4.64	4.29	1.74	8.32	8.03
CaO	8.46	8.33	8.00	7.89	7.87	7.82	3.47	7.68	7.45
Na_2O	3.47	3.68	3.78	4.21	4.52	4.47	3.04	4.59	4.55
K_2O	0.74	0.79	0.94	1.03	1.11	1.10	4.10	2.82	2.54
P_2O_5	0.14	0.17	0.20	0.22	0.24	0.22	0.11	1.37	0.90
H_2O^+	0.34	0.21	0.25	0.22	0.24	0.18	0.62	1.00	0.43
H_2O^-	0.10	0.10	0.10	0.10	0.12	0.08	0.20	0.19	0.04
Total	99.64	99.77	99.96	99.78	99.47	99.74	99.47	99.11	99.87
Mg#	0.73	0.72	0.70	0.68	0.66	0.68	0.52	0.80	0.80
CIPW Norm (wt%)									
qz	–	–	–	3.07	0.60	2.50	23.85	–	–
or	4.41	4.69	5.58	6.12	6.62	6.53	24.56	17.01	15.10
ab	29.60	31.31	32.11	35.82	38.59	38.02	26.08	27.90	33.86
an	27.32	27.25	26.91	28.26	27.81	28.87	12.76	9.99	13.41
ne	–	–	–	–	–	–	–	6.37	2.64
di	11.32	10.61	9.37	7.73	8.06	6.93	3.25	15.55	14.02
hy	14.20	15.02	17.95	12.58	12.38	10.27	5.96	–	–
fo	6.36	4.64	2.32	–	–	–	–	10.01	9.74
fa	2.65	1.96	1.08	–	–	–	–	0.62	0.56
mt	2.28	2.45	2.30	4.02	3.61	4.55	2.06	6.72	6.24
il	1.55	1.68	1.91	1.89	1.76	1.81	1.23	2.58	2.33
ap	0.33	0.40	0.47	0.51	0.56	0.51	0.26	3.25	2.10

Analyses: I.S.E. Carmichael and J. Hampel. Jor 44, 31, 1A, 7, 11, and 28 from Jorullo eruption. LHG = La Huacana Granite, Jor 46 and 46d from Cerro La Pilita. Stage – E (early), M (middle), L (late) stages of the Jorullo eruption. $Mg\# = Mg/Mg + Fe^{+2}$, calculated using analyzed FeO

Table 2. Instrumental-neutron-activation analyses of whole-rock samples (ppm)

Jor	44		11		46		46d	
Sc	27.85	(0.06)	19.11	(0.04)	18.11	(0.04)	17.64	(0.04)
Cr	516	(6)	75	(1)	338	(3)	278	(3)
Mn	1,042	(20)	872	(17)	883	(16)	851	(17)
Co	42.8	(0.6)	25.0	(0.4)	41.9	(0.6)	30.0	(0.4)
Cs	0.57	(0.23)	0.39	(0.17)	<0.8		<0.7	
Ba	221	(13)	355	(12)	1,222	(24)	1,160	(52)
La	7.9	(0.6)	12.6	(0.5)	91.5	(1.1)	68.6	(1.4)
Ce	18.3	(0.4)	29.4	(0.2)	172	(2)	131	(2)
Nd	10.0	(0.9)	17	(1)	67	(3)	53	(2)
Sm	2.65	(0.03)	3.39	(0.03)	7.79	(0.08)	6.71	(0.02)
Eu	0.90	(0.01)	1.12	(0.06)	2.04	(0.02)	1.79	(0.02)
Tb	0.48	(0.01)	0.48	(0.03)	0.62	(0.02)	0.56	(0.02)
Dy	3.11	(0.15)	2.94	(0.14)	2.68	(0.14)	2.90	(0.12)
Yb	1.95	(0.02)	1.70	(0.05)	1.25	(0.04)	1.18	(0.04)
Lu	0.26	(0.02)	0.22	(0.01)	0.17	(0.02)	0.20	(0.02)
Hf	2.44	(0.04)	3.46	(0.15)	5.60	(0.09)	4.57	(0.09)
Th	0.73	(0.07)	1.14	(0.06)	5.19	(0.07)	3.98	(0.07)
U	0.29	(0.02)	0.39	(0.02)	1.18	(0.03)	0.86	(0.03)
Ta	0.136	(0.002)	0.24	(0.04)	0.960	(0.001)	0.694	(0.006)
Eu/Eu*	0.99		1.02		0.93		0.94	

Numbers in parentheses represent counting uncertainties of one standard deviation
Eu* is interpolated between chondrite-normalized (Masuda et al. 1973) values for Sm and Tb
INA analyses by F. Asaro and H. Michel, Lawrence Berkeley Laboratory (Perlman and Asaro 1969)

Table 3. Trace element analyses (ppm) of whole-rock samples by X-ray fluorescence

Jor	44	31	1A	7	11	28	LHG	46	46d
V	186	210	202	186	216	213	107	217	228
Cr	564	441	320	98	105	52	10	338	329
Ni	261	200	152	51	44	26	2	248	221
Cu	60	54	46	40	35	31	43	72	98
Zn	61	64	63	66	66	77	59	172	136
Ga	16	18	16	21	18	22	14	25	27
Rb	10	12	16	14	16	16	204	17	19
Sr	397	452	478	585	615	622	135	2,250	1,984
Y	20	21	20	20	21	18	32	18	18
Zr	100	109	126	127	130	136	251	203	183
Nb	12	12	12	15	9	13	14	24	21
Ba	204	231	262	314	352	330	537	1,271	1,130
La	9	7	13	13	9	13	28	98	74
Ce	18	20	22	23	28	34	52	158	130

Energy dispersive XRF analyses of undiluted pressed powder pellets at UCB

Uncertainties of one standard deviation are equal to the following percentages of the amounts present: V (8%), Cr (10%), Ni (15%), Cu (12%), Zn (10%), Ga (10%), Rb (10%), Sr (5%), Y (15%), Zr (5%), Nb (10%), Ba (3%), La (15%), and Ce (10%)

cates the strong light REE enrichment of the Cerro la Pilita trachybasalts compared to the lavas from Jorullo.

Petrography and mineralogy

Textures and modes

The early lavas of Jorullo, represented by Jor 44, are porphyritic basalts with 5–6 vol% olivine phenocrysts containing Cr–Al–Mg spinel inclusions, and microphenocrysts of olivine, plagioclase, and augite, in a hyaloophitic to intersertal groundmass (Williams et al. 1982) consisting of plagioclase laths, small grains of augite, olivine, and spinel, and 10–40 vol% brown glass (Table 4). Progressing to younger, more-silicic samples, the proportion of olivine decreases whereas the amounts of plagioclase and augite increase. The late lavas from the main cone of Jorullo (Jor 7, 11, 28) usually show relict phenocrysts and microphenocrysts of hornblende, or rarer microphenocrysts and groundmass crystals of orthopyroxene.

The trachybasalts from Cerro La Pilita have phenocrysts of olivine, augite, and hornblende, probable xenocrysts of anhedral, sieve-textured plagioclase, and microphenocrysts of the same phases plus apatite, enclosed in an intergranular matrix having plagioclase > spinel > augite > olivine > apatite (Table 4).

Mineralogy

Olivine

Magnesian olivine crystals up to 4 mm across occur in every sample from Jorullo and Cerro La Pilita. Most crystals are euhedral, although subhedral and skeletal forms are also present. Some olivine microphenocrysts are inclusion-free, but most larger crystals have from a dozen to over 60 small (<15 micron) included cubes of orange-brown spinel (Fig. 4). These tend to occur in strings or clusters, giving the appearance of a single spinel crystal up to 120 microns across. Several small olivine crystals show up to 25% of their cross-sectional area occupied by these large spinel clusters, but usually the clusters represent no more than a few percent of the host olivine volume. Some olivine phenocrysts have groundmass-filled re-entrants or small (<15 micron) glass inclusions with contraction bubbles.

Fig. 5 shows histograms of Mg-numbers in olivines. Phenocryst cores range from Fo_{86} to Fo_{90} in the early lavas of Jorullo and from Fo_{73} to Fo_{87} in the late, main-cone lavas. Phenocryst rims and groundmass crystals are more Fe-rich, reaching Fo_{79} and Fo_{69} in the early- and late-stage lavas, respectively. NiO varies sympathetically with MgO in the Jorullo olivines, ranging from 0.43 to 0.03 wt%. In Jor 46 from Cerro La Pilita, olivine crystals are also normally zoned, with cores ranging from Fo_{85} to Fo_{88} and rims ranging from Fo_{82} to Fo_{87} (Fig. 5).

Table 4. Modes determined by point counting (vol%)

		points	oliv	plag	cpx	opx	hbd	spin	xlls	grnd
44	ph	1,257	5.8	–	–	–	–	–	8.9	91.1
	mp		1.4	1.1	0.5	–	–	0.1		
31	ph	1,359	5.4	0.3	–	–	–	–	17.2	82.8
	mp		0.9	9.4	1.0	–	–	0.2		
1A	ph	1,321	5.7	0.5	0.1	–	–	–	31.9	68.1
	mp		0.5	11.6	12.7	–	–	0.8		
7	ph	1,278	1.0	–	0.2	–	–	–	26.5	73.5
	mp		0.1	22.7	2.3	0.2	–	–		
11	ph	1,287	0.4	0.4	–	–	0.1	–	9.5	90.5
	mp		1.3	6.3	0.2	tr	0.8	–		
28	ph	1,234	0.2	0.6	–	–	0.1	–	10.2	89.8
	mp		0.3	8.5	0.2	tr	0.3	–		
46	ph	1,432	5.9	0.6	0.6	–	0.1	–	19.9	80.1
	mp[a]		2.3	2.3	5.9	–	1.0	1.0		
46d	ph	1,346	8.3	–	0.2	–	–	–	15.6	84.4
	mp		1.4	0.7	3.4	–	1.3	0.3		

points = points counted, *oliv* = olivine, *plag* = plagioclase, *cpx* = clinopyroxene, *opx* = orthopyroxene, *hbd* = hornblende, *spin* = spinel, *xlls* = all crystals, *grnd* = groundmass

Following Wilcox (1954): *ph* = phenocrysts (>0.3 mm), *mp* = microphenocrysts (<0.3 mm and >0.03 mm), *grnd* = groundmass (glass plus crystals <0.03 mm)

[a] sample 46 contains 0.2 vol% microphenocrystic apatite

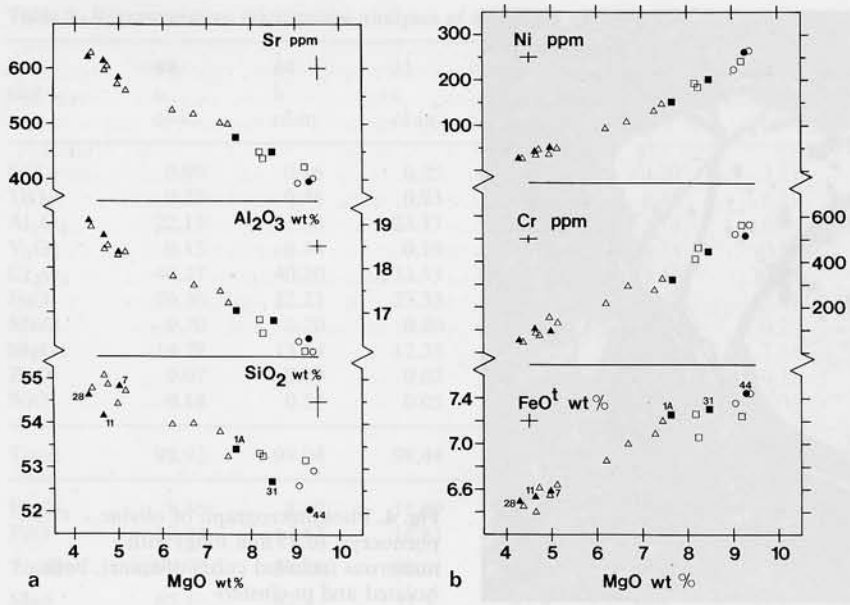

Fig. 2a and b. MgO variation diagrams for 20 Jorullo lava samples. Circles = early-stage samples, squares = middle-stage samples, triangles = late-stage samples. Closed symbols represent analyses from Table 1, open symbols are analyses from Appendix 1. Error crosses indicate estimated 1 sigma variations for XRF data

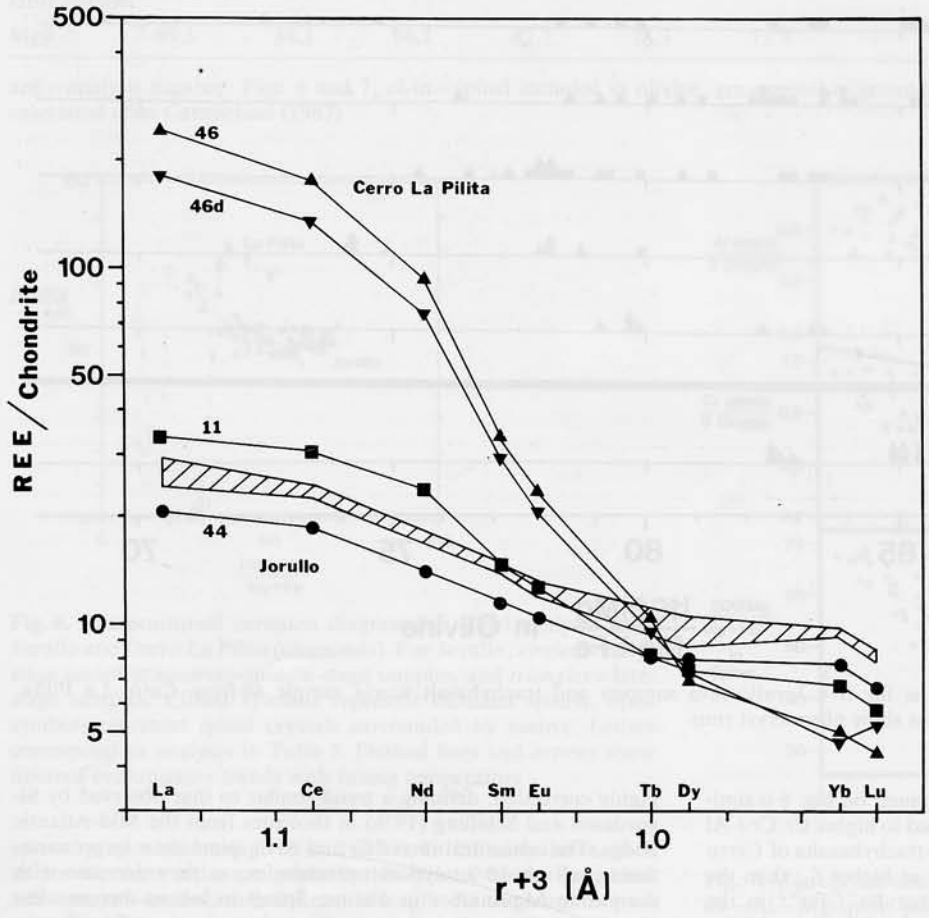

Fig. 3. Chondrite-normalized rare earth element plot of data from Table 2. Diagonally ruled field shows predicted REE pattern for Jor 11 based on the model in Table 10. Chondritic values from Masuda et al. (1973). Ionic radii from Whittaker and Muntus (1970)

Spinel

Orange-brown cubes of spinel occur primarily as inclusions within olivine crystals, but can also be found as isolated crystals and clusters in the groundmasses. These groundmass clusters are identical to clusters within olivine crystals. Representative microprobe analyses of spinels are given in Table 5, and a larger number of analyses are plotted on Figs. 6 and 7. Spinels included in the most Mg-rich olivines of the early-stage Jor 44 are the richest in Cr, Al, and Mg, and as the eruption evolved, spinels became depleted in these elements and enriched in Fe and Ti. The ratio Cr/Cr + Al shows little variation during this evolution (Fig. 6). Most Cr-rich spinels in the groundmasses have thin 2 micron) rims of titanomagnetite, which also forms independent grains in the groundmasses of late-stage Jorullo lavas (Table 5). The inferred evolutionary path of the Jorullo spinels is indicated by arrows in Fig. 6.

Sample Jor 46 also contains two spinels, Cr – Al – Mg-rich inclusions in olivines and Cr-poor groundmass titanomagnetites.

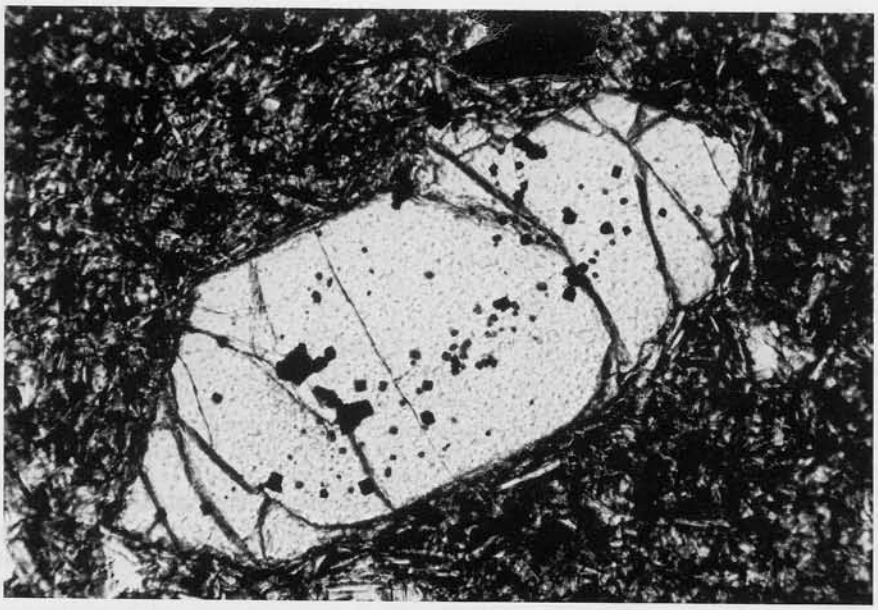

Fig. 4. Photomicrograph of olivine phenocryst (0.85 mm long) with numerous included cubes of spinel, both isolated and in clusters

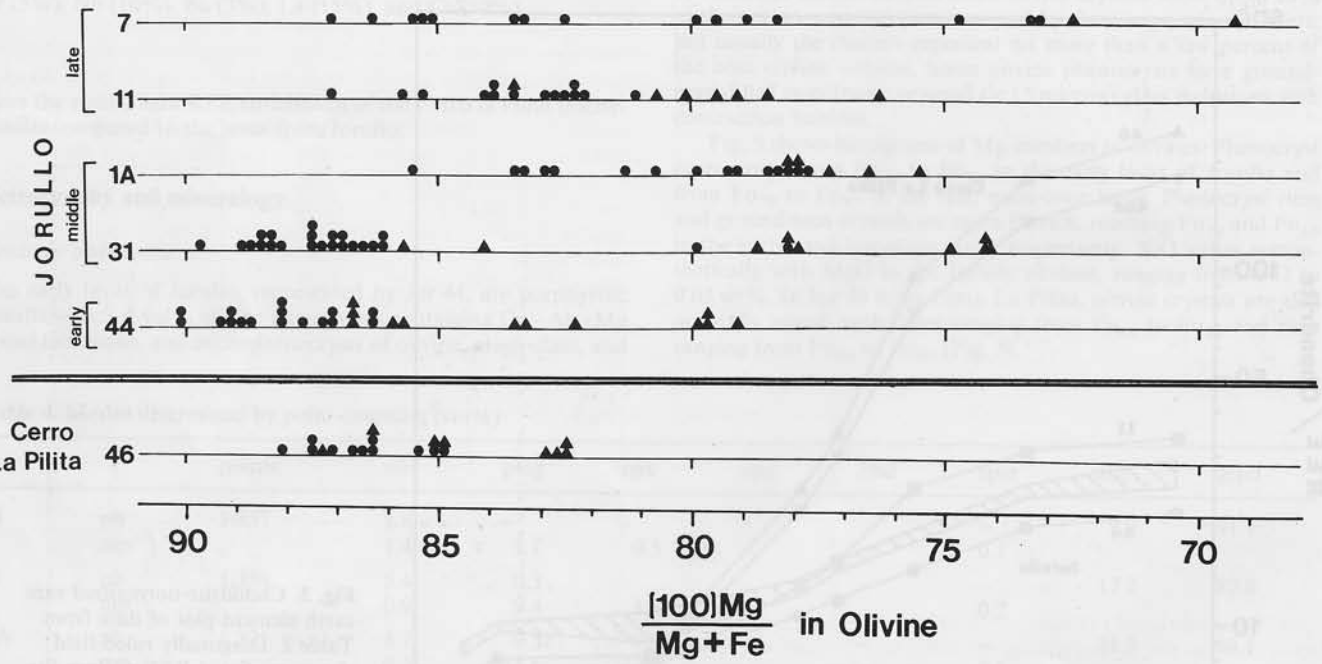

Fig. 5. Histograms of Mg-number in olivine for five Jorullo lava samples and trachybasalt scoria sample 46 from Cerro La Pilita. Dots represent phenocryst cores and triangles show phenocryst rims

The compositional evolution path of these spinels on Fig. 6 is similar to that for the Jorullo spinels, but displaced to higher $Cr/Cr+Al$ and $Mg/Mg+Fe^{+2}$. As discussed later, the trachybasalts of Cerro La Pilita were probably more hydrous and at higher f_{O_2} than the Jorullo basalts. The higher f_{O_2} led to higher Fe^{+3}/Fe^{+2} in the melt and higher Mg/Fe^{2+} in all minerals, resulting in a higher Mg-number at the Cr-spinel to titanomagnetite transition (Fig. 6).

In order to document the co-variation of olivine and spinel compositions through the Jorullo eruptive sequence, host-inclusion pairs were carefully analyzed. Spinels were chosen only if completely enveloped by olivine in the plane of the section. Each olivine analysis was taken on the side of the spinel inclusion closest to the olivine core. Over 65 high-quality olivine-spinel analyses were obtained from the Jorullo lavas. In Fig. 7, the host olivine Mg-number is plotted against the Mg-number and Cr and Al contents of its included spinel. The Mg-numbers of spinel and olivine are highly correlated, defining a trend similar to that observed by Sigurdsson and Schilling (1976) in tholeiites from the Mid-Atlantic Ridge. The concentrations of Cr and Al in spinel show larger variations, well above analytical uncertainties, as they decrease with decreasing Mg-number in olivine. Spinel inclusions become less abundant as host olivine compositions become more Fe-rich; the most-evolved $Cr-Al-Mg$-spinels occur in olivines of Fo_{73} composition (Fig. 7). The relatively abrupt transition to titanomagnetite as the dominent spinel phase apparently occurs at a slightly more Fe-rich olivine composition.

Plagioclase

The groundmasses of all Jorullo lavas are dominated by innumerable plagioclase laths with inconsistent rim-to-core compositional zoning in the range An_{75} to An_{50}. Representative microprobe anal-

Table 5. Representative microprobe analyses of spinels

Jor	44	44	31	11	1A	7	1A	7	46	46
an#	a	b	c	d	e	f	g	h	i	j
	ol-in	ol-in	ol-in	ol-in	ol-in	ol-in	gm	gm	ol-in	gm
SiO_2	0.09	0.16	0.25	0.35	0.20	0.21	0.16	0.21	0.07	0.17
TiO_2	0.55	0.46	0.93	1.81	1.42	1.21	6.24	14.94	1.57	8.11
Al_2O_3	22.13	21.68	23.17	17.97	15.18	16.48	7.08	2.24	10.60	3.22
V_2O_5	0.13	0.14	0.19	0.26	0.24	0.16	0.45	0.77	0.30	0.14
Cr_2O_3	40.27	40.30	33.55	29.78	29.41	30.13	22.40	0.83	40.97	0.22
FeO	20.56	22.23	27.33	37.69	42.87	42.47	54.24	72.90	33.14	75.60
MnO	0.20	0.20	0.20	0.24	0.30	0.25	0.34	0.35	0.26	0.48
MgO	14.79	13.64	12.75	10.41	7.94	7.35	6.35	3.37	10.47	6.59
ZnO	0.07	0.09	0.02	0.09	0.10	0.11	0.06	0.12	0.02	0.08
NiO	0.14	0.14	0.05	0.06	0.10	0.06	0.10	0.00	0.06	0.05
Total	98.93	99.04	98.44	98.66	97.76	98.43	97.42	95.73	97.46	94.66
Fe_2O_3	8.46	8.40	11.69	19.02	22.06	20.28	28.66	36.84	16.44	52.25
FeO	12.94	14.67	16.81	20.57	23.02	24.22	28.44	39.75	18.34	28.58
Total	99.77	99.88	99.61	100.56	99.97	100.46	100.28	99.42	99.10	99.89
Mg#	67.1	62.4	57.5	47.4	38.1	35.1	28.5	13.1	50.4	29.1
Host olivine:										
Mg#	89.3	88.1	86.1	82.2	78.3	73.3	–	–	86.5	–

an# = analysis number: Figs. 6 and 7; ol-in = spinel included in olivine, gm = spinel in groundmass; Mg# = 100 ($Mg/Mg+Fe^{+2}$); Fe_2O_3 calculated after Carmichael (1967)

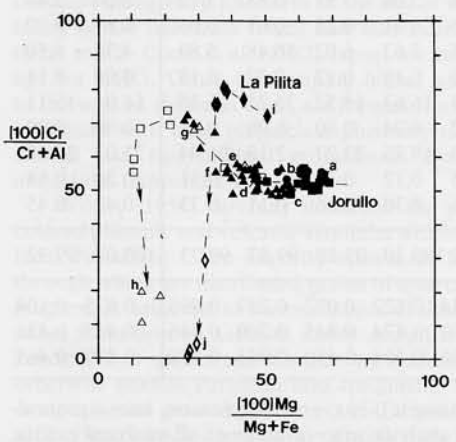

Fig. 6. Compositional variation diagram for spinel analyses from Jorullo and Cerro La Pilita (diamonds). For Jorullo: *circles* = early-stage samples, *squares* = middle-stage samples, and *triangles* = late-stage samples. Closed symbols represent included spinels, open symbols represent spinel crystals surrounded by matrix. Letters correspond to analyses in Table 5. Dashed lines and arrows show inferred evolutionary trends with falling temperature

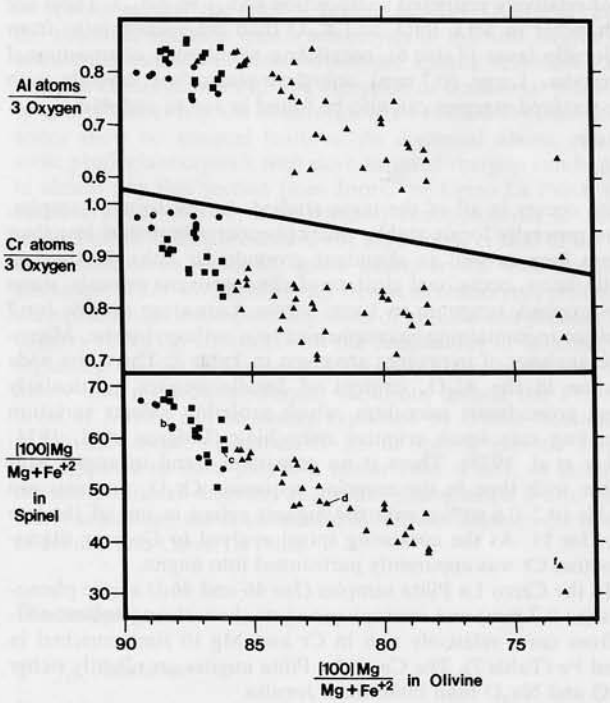

Fig. 7. Microprobe analyses of coexisting host olivine and included Cr – Al – Mg-spinel pairs from Jorullo lavas. *Circles* = early-stage samples, *squares* = middle-stage samples, and *triangles* = late-stage samples. Letters correspond to spinel analyses in Table 5

yses of plagioclases are given in Table 6. In the early lavas, such as Jor 44, these laths are generally less than 0.03 mm long, but a few narrow blades reach 0.4 mm in length. As the eruption progressed, the successively more-evolved lavas carried larger and more abundant plagioclase crystals with a greater range in composition. The late, hornblende-bearing lavas Jor 11 and 28 contain euhedral-subhedral plagioclase phenocrysts greater than 1 mm across, including both crystals with glass-inclusion-riddled cores and others that are inclusion-free in the plane of the section. Phenocrysts are both normally zoned and reversely zoned, with a wide compositional range represented in each thin section (An_{85} to An_{35}). The late, orthopyroxene-bearing lava sample Jor 7 is exceptional in having no plagioclase crystals larger than 0.1 mm; most of these plagioclase microphenocrysts are normally zoned, also in the range An_{85} to An_{35}. The later lavas of Paricutin are also characterized by a lack of plagioclase phenocrysts (Wilcox 1954).

Almost any thin section of a Jorullo lava contains one or two large (up to 1 mm) anhedral plagioclase crystals with glass-inclusion riddled, sieve-textured margins commonly surrounding relatively sodic cores (An_{45}). As discussed below, these are probably xenocrysts derived from digestion of granitic or volcanic

Table 6. Representative microprobe analyses of plagioclase cores and rims

Jor	44 mp-c	44 mp-r	31 mp-c	31 mp-r	7 mp-c	7 mp-r	1A ph-c	1A ph-r	11 mp-c	11 mp-r	46 mp-c	46 mp-r
SiO_2	49.28	51.26	49.93	50.43	48.97	51.22	54.93	56.76	48.44	48.47	55.46	55.61
Al_2O_3	31.36	30.14	30.67	30.71	32.16	29.70	28.18	26.67	32.49	32.04	26.00	26.25
Fe_2O_3	0.79	0.96	0.77	0.77	0.64	0.89	0.90	0.51	0.60	0.70	0.96	1.09
BaO	0.01	0.00	0.00	0.00	0.00	0.08	0.04	0.02	0.02	0.00	0.47	0.35
CaO	15.15	13.70	14.21	14.37	15.22	12.83	10.74	9.28	15.19	15.29	8.08	8.18
SrO	0.19	0.36	0.32	0.17	0.30	0.37	0.23	0.12	0.38	0.22	1.70	1.70
Na_2O	2.86	3.61	3.19	3.17	2.59	4.15	5.22	6.02	2.68	2.86	5.83	5.72
K_2O	0.06	0.12	0.07	0.08	0.08	0.24	0.25	0.37	0.07	0.05	0.84	0.73
Total	99.70	100.15	99.16	99.70	99.96	99.48	100.49	99.75	99.87	99.63	99.34	99.63
X_{Ca}	0.742	0.673	0.708	0.711	0.761	0.622	0.524	0.450	0.755	0.745	0.412	0.421
X_{Na}	0.254	0.320	0.288	0.284	0.234	0.364	0.461	0.529	0.241	0.252	0.537	0.534
X_K	0.004	0.007	0.004	0.005	0.005	0.014	0.015	0.021	0.004	0.003	0.051	0.045

ph/mp = phenocryst/microphenocryst, r/c = rim/core

country-rocks, but may also represent plagioclase crystals formed at relatively high pressure and later resorbed prior to eruption. The sieve-textured margins of these crystals look little different from the glass-inclusion-riddled cores of euhedral phenocrysts in the late Jorullo lavas, and these phenocrysts may have grown over xenocrystic cores.

Samples Jor 46 and 46d from Cerro La Pilita have groundmasses dominated by plagioclase laths ranging up to 0.15 mm long, but of relatively restricted composition (An_{42} to An_{40}). These are much richer in SrO, BaO, and K_2O than plagioclase laths from the Jorullo lavas (Table 6), paralleling whole-rock compositional differences. Large (0.7 mm) anhedral plagioclase crystals with sieve-textured margins can also be found in Jor 46 and 46d.

Augite

Augite occurs in all of the lavas studied. In the Jorullo samples, augite generally forms stubby microphenocrystic prisms less than 0.2 mm long as well as abundant groundmass laths. In the late Jorullo lavas, occasional clusters of clinopyroxene crystals, some sieve-textured, range up to 1 mm across. Late-stage sample Jor 7 is unique in containing microphenocrystic orthopyroxene. Microprobe analyses of pyroxenes are given in Table 7. There is a wide variation in the Al_2O_3 content of Jorullo augites, particularly among groundmass microlites, which probably reflects variation in cooling rate upon eruptive quenching (Lofgren et al. 1974; Walker et al. 1978). There is no consistent trend in augite Mg-number with time in the eruption sequence. Cr_2O_3 contents are variable (0.2–0.6 wt%), with the highest values in one of the late lavas, Jor 11. As the coexisting spinel evolved to Cr-poor titanomagnetite, Cr was apparently partitioned into augite.

In the Cerro La Pilita samples (Jor 46 and 46d) augite phenocrysts (to 0.7 mm) and microphenocrysts show strong optical zoning from cores relatively rich in Cr and Mg to rims enriched in Ti and Fe (Table 7). The Cerro La Pilita augites are slightly richer in SrO and Na_2O than those from Jorullo.

Hornblende

Late lavas from Jorullo show hornblende pseudomorphs up to 1 mm across, consisting primarily of opacite (fine-grained magnetite). Fresh brown hornblende cores can occasionally be found and several inclusions of pristine hornblende were seen within olivine phenocrysts. These late-stage Jorullo hornblende crystals are also rich in Cr_2O_3, apparently for the same reason discussed for augite.

Orange-yellow-brown hornblende is also a common phenocrystic (to 0.5 mm) and microphenocrystic phase in the Cerro La Pilita samples. In the quickly quenched scoria sample Jor 46, hornblende forms fresh euhedral crystals, whereas it has largely reacted to opacite in the lava sample Jor 46d: additional evidence that the reaction of hornblende to opacite occurs during lava extrusion (Kuno 1950; Luhr and Carmichael 1980). Representative microprobe analyses of hornblendes are given in Table 8. The Cerro La Pilita hornblendes are richer in TiO_2, SrO, K_2O, and F than those from Jorullo.

Table 7. Representative microprobe analyses of pyroxenes

Jor	44 cpx micr	31 cpx micr	1A cpx avg	7 cpx avg	7 opx avg	11 cpx avg	46 cpx ph-c	46 cpx ph-r
SiO_2	49.80	52.92	52.54	50.96	54.07	50.98	52.45	51.07
TiO_2	0.90	0.44	0.73	0.66	0.46	0.61	0.53	0.86
Al_2O_3	4.75	1.71	2.06	3.58	0.88	3.72	2.04	2.44
Cr_2O_3	0.32	0.36	0.41	0.28	0.01	0.63	0.61	0.02
FeO	6.43	8.05	7.63	6.02	16.48	5.89	4.71	6.50
MnO	0.13	0.20	0.18	0.12	0.37	0.13	0.08	0.11
MgO	15.08	19.18	16.63	15.52	25.21	15.38	16.01	15.11
NiO	0.00	0.02	0.04	0.00	0.00	0.01	0.00	0.00
CaO	22.26	17.43	19.75	22.27	2.18	21.94	23.02	22.62
SrO	0.12	0.15	0.12	0.11	0.10	0.11	0.20	0.14
Na_2O	0.32	0.26	0.30	0.36	0.11	0.33	0.42	0.45
Total	100.11	100.72	100.39	99.88	99.87	99.73	100.07	99.32
X_{Fe}	0.104	0.124	0.122	0.097	0.257	0.096	0.075	0.104
X_{Mg}	0.435	0.530	0.474	0.445	0.700	0.446	0.455	0.431
X_{Ca}	0.461	0.346	0.404	0.458	0.043	0.458	0.470	0.465

cpx = clinopyroxene (augite), *opx* = orthopyroxene, *micr* = groundmass microlite point analysis, *avg* = average of all analyzed points, *ph-r*/*ph-c* = phenocryst rim/core

Apatite

F–Sr-rich apatite forms occasional microphenocrystic and groundmass prisms in the trachybasalts from Cerro La Pilita (Jor 46, 46d). The average microprobe analysis is given in Table 8.

Country rocks and xenoliths

Tertiary granites and granodiorites can be found in many places in the southern Michoacán-Guanajuato Volcanic Field, including

Table 8. Average microprobe analyses of hornblende phenocrysts and apatite

Jor	11 hornblende	46 hornblende	46 apatite
SiO_2	42.73	41.65	0.55
TiO_2	2.48	3.18	nd
Al_2O_3	13.26	11.47	0.01
Cr_2O_3	0.73	0.02	nd
FeO	8.14	9.44	0.26
MnO	0.06	0.07	nd
NiO	0.10	0.01	nd
MgO	15.95	15.44	0.37
BaO	0.00	0.06	0.00
CaO	11.92	11.88	55.20
SrO	0.05	0.16	0.53
Na_2O	2.63	2.71	0.25
K_2O	0.26	1.44	0.00
P_2O_5	0.00	0.03	40.57
F	0.05	0.25	1.90
Cl	0.02	0.01	0.15
$-O=F+Cl$	0.02	0.11	0.83
Total	98.36	97.71	98.96

nd = not determined

Table 9. Olivine-melt liquidus temperatures and oxygen fugacities

Jor	44	31	1A	7	11	46
max Mg#	90.5	89.7	85.4	87.1	87.0	88.2
Temperatures (°C)						
T_{RE}	1,230	1,205	1,185	1,090	1,070	1,190
T_{exp} (1-atm)						
OLIV	1,260	–	1,220	1,190	–	1,240
PLAG	1,190	–	1,190	1,220	–	1,180
$-\log f_{O_2}$	6.88	7.02	7.46	7.14	7.79	4.75
(Ni−NiO)	(7.50)	(7.78)	(8.01)	(9.19)	(9.46)	(7.95)

T_{RE} = temperatures obtained from olivine saturation surface plot (Fig. 7) of Roeder and Emslie (1970) using whole-rock analyses (Table 1)
T_{exp} = liquidus temperatures for olivine and plagioclase at 1 atm with f_{O_2} buffered by Ni−NiO (Mo and Carmichael, unpublished data)
$-\log f_{O_2}$ = calculated from egn 9 in Sack et al. (1980) at T_{RE} using whole-rock compositions and measured $Fe^{+3}/(Fe^{+3}+Fe^{+2})$ (Table 1)
(Ni−NiO) = values of $-\log f_{O_2}$ for Ni−NiO buffer (Eugster and Wones 1962) at T_{RE}

exposures within 30 km of Parícutin and directly adjacent to Volcán del Sur at Jorullo. La Huacana Granite, named for prominent outcrops along Hwy 120 north of the city of the same name, forms many of the basement ridges and hills near Jorullo, particularly to its south. Clark et al. (1982) report an early Oligocene K−Ar age for LHG. Other topographic highs, such as Cerro Partido to the west of the main cone, are formed from a strongly porphyritic basalt with large plagioclase phenocrysts (to 5 mm) set in an altered and recrystallized groundmass containing quartz-filled amygdules (Appendix 2).

Wilcox (1954) carefully described the petrography of light-colored plutonic and volcanic xenoliths within the lavas and bombs from Parícutin; "The majority consist of highly vesicular glass through which are distributed grains of quartz, feldspar, and ferromagnesian minerals in various stages of destruction". Transition zones from lava to xenolith rarely exceed a few millimeters, but xenocrysts of quartz and feldspar are occasionally encountered in otherwise normal Parícutin lava specimens. On petrographic and compositional grounds, Wilcox (1954) argued that assimilation of salic country rock operated in concert with fractional crystallization of olivine and plagioclase to generate the compositional evolution from early basaltic andesite to late andesite at Parícutin.

La Huacana Granite[a], where sampled about 6 km north of the city (Fig. 1), has a subhedral granular texture with 37 vol% plagioclase, 29% K-feldspar, 22% quartz, 5% augite, 2% brown biotite, 5% secondary green-brown mica, and lesser amounts of orthopyroxene, titanomagnetite, ilmenite, and zircon. It is nearly identical petrographically to the granodiorite studied by Wilcox (1954) from the Parícutin area. Granitic xenoliths also occur in Jorullo lavas, particularly those from the middle-stage satellite cones to the NE and SW of the main cone. The protoliths were very similar to the studied specimen of La Huacana Granite, and xenolith textures closely match those described from Parícutin (Wilcox 1954). In the Jorullo case, the xenolith margins are also very sharp, and their interiors show the original plutonic minerals dispersed within light-colored vesicular glass. Quartz and feldspar are commonly shattered and dusty with minute inclusions. Patches of opacite occupy the sites of former biotites. Quartz crystals in the xenoliths and rare quartz xenocrysts in the host basalts show undulatory extinction. Host basalts are usually vesiculated along xenolith contacts, but with the exception of occasional plagioclase or quartz xenocrysts, the basalts just a few millimeters from contact zones show no unusual features. As discussed above, relatively sodic plagioclase crystals with sieve-textured margins can be found in almost any thin section from Jorullo or Cerro La Pilita. Other exotic crystals include: sieve-textured clinopyroxenes in Jor 7, a single Fe-rich orthopyroxene in Jor 31, a single crystal of the pseudobrookite series in Jor 11, and a quartz crystal with undulatory extinction in Jor 46. These are all viewed as xenocrysts, presumably derived through incomplete digestion of granitic and perhaps other country rocks. In contrast with the conclusions of Wilcox (1954) regarding magma evolution at Parícutin, however, we will argue below that most compositional variations among the 1759–1774 lavas of Jorullo can be simply explained by crystal fractionation of olivine + augite + plagioclase + minor spinel; granitic assimilation appears to have played a minor role, if any, in generating the compositional diversity at Jorullo. Assimilation is also incapable of explaining the fundamental differences between the magmas of Jorullo and Cerro La Pilita.

[a] With plag:kspar:qtz as 42:33:25, LHG qualifies as a granite in the classification of Streckeisen (1974). The SiO_2 content of LHG (67.2 wt%), however, is rather low for a granite. Four other analyses of basement plutonic rocks (App. 2) range from 63.5 to 76.0% SiO_2. In this paper we loosely refer to all of these rocks as granites

Discussion

$T-f_{O_2}$ relations

Liquidus temperatures for the Jorullo lavas can be estimated from experimental calibrations of the distribution of Mg and Fe^{+2} between olivine and silicate melt (Roeder and Emslie 1970). Temperatures calculated using the most Mg-rich olivine composition in each sample and the whole-rock analysis are listed in Table 9 (T_{RE}), indicating a steady decrease in liquidus temperature through the course of the eruption from 1,230° C in early-stage Jor 44 to 1,070° C in late-stage Jor 11. Table 9 also gives experimentally determined 1-atm liquidus temperatures for olivine and plagioclase in four of the bulk compositions (Mo and Carmichael,

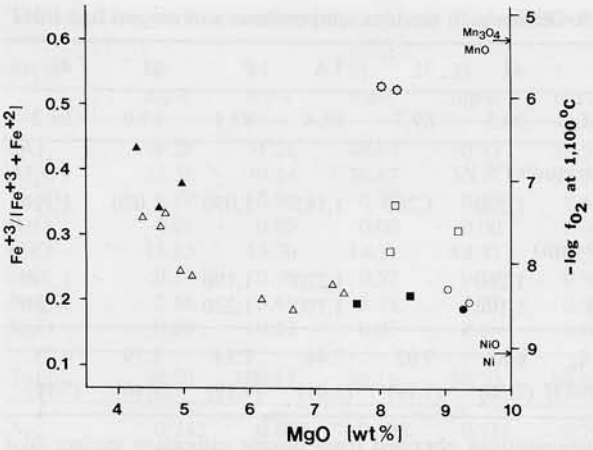

Fig. 8. Assuming that measured ferric-ferrous ratios reflect magmatic conditions, whole-rock values of $Fe^{+3}/(Fe^{+3}+Fe^{+2})$ are plotted versus whole rock MgO. Values of $-\log f_{O_2}$ were calculated at 1,100° C following Sack et al. (1980). $MnO-Mn_3O_4$ buffer from Huebner (1969) and Ni–NiO buffer from Eugster and Wones (1962). *Circles* = early-stage samples, *squares* = middle-stage samples, *triangles* = late-stage samples. Closed symbols represent analyses from Table 1, open symbols are analyses from Appendix 1. Open star symbols represent trachybasalts from Cerro La Pilita

unpublished data). The calculated liquidus temperature is just 30° C lower than the 1-atm olivine liquidus temperature for the early-stage lava Jor 44 (1,260° C), but calculated temperatures are steadily lower than the 1-atm liquidus values for middle-stage Jor 1A and late-stage Jor 7. This divergence is consistent with progressively higher concentrations of H_2O and other volatiles in the more silica-rich Jorullo magmas, acting to depress all melting temperatures.

Late-stage sample Jor 7, from the main Jorullo cone, is the only sample containing orthopyroxene as well as augite. Average pyroxene compositions listed in Table 7 were used to calculate eruptive temperatures of 985° C and 1,000° C from the pyroxene geothermometers of Wood and Banno (1973) and Wells (1977), respectively. These values are consistent with the presence of hornblende in other late-stage lavas, given the upper thermal stability limits for amphiboles in andesites (950° C) and basalts (1,050° C) determined experimentally (Eggler 1972; Eggler and Burnham 1973; Allen et al. 1975; Allen and Boettcher 1978 and 1983). The calculated olivine-melt liquidus temperature for Jor 7 is sensibly higher than the calculated pyroxene quench temperatures.

Sack et al. (1980) experimentally calibrated the ferric-ferrous ratio of silicate melts as a function of T, f_{O_2}, and melt composition. This calibration can be used to calculate f_{O_2} when the other variables are known. The ferric-ferrous ratio has the greatest influence on calculated f_{O_2}. Fig. 8 is a plot of MgO versus $Fe^{+3}/(Fe^{+3}+Fe^{+2})$ and $-\log f_{O_2}$ at 1,100° C for the 20 whole-rock samples from the Jorullo eruption (Table 1 and Appendix 1). Many samples from all stages of the eruption have relatively low $Fe^{+3}/(Fe^{+3}+Fe^{+2})$ in the range 0.18 to 0.25, corresponding to oxygen fugacities 0.5 to 1.0 log units above the Ni–NiO buffer. Higher values are shown by three middle-stage samples and the most Mg-poor, late-stage samples, which yield f_{O_2} values 1.5 to 2.5 log units above Ni–NiO. These wide variations in ferric-ferrous ratio and calculated oxygen fugacity might be viewed as the result of secondary oxidation and alteration of the glass, but no other evidence can be presented to support this notion. On the contrary, we suggest that these values reflect pre-eruptive magmatic conditions. Evidence has been cited for strong interaction of magma and groundwater during the early, phreatomagmatic phase of the Jorullo eruption (Sept 29 to Oct 14, 1759). This interaction may have led to variable increases in the oxidation state of the magma; only the ferric-ferrous ratio of the melt phase may have been responsive enough to record this event. Oxygen fugacities at calculated liquidus temperatures (T_{RE}) are also listed for the samples in Table 9.

The same olivine-melt geothermometer was used to calculate a liquidus temperature of 1,190° C for trachybasalt Jor 46 from Cerro La Pilita (Table 9). The presence of hornblende in the trachybasalts indicates an eruption temperature of 1,050° C or less. The liquidus temperature (T_{RE}) and the analyzed ferric-ferrous ratio were used to calculate f_{O_2} (Sack et al. 1980), which lies 3.2 log units above Ni–NiO. Similarly high f_{O_2} values have been calculated for other basic alkaline magmas containing hydrous phenocrysts using the same method (Luhr and Carmichael 1981).

Olivine-spinel equilibria

Experimental studies at 1 atm pressure using natural basalt compositions have shown that spinel is the liquidus phase followed by olivine for f_{O_2} values above the Ni–NiO buffer, and that olivine precedes spinel under more reducing conditions (Roeder and Emslie 1970; Hill and Roeder 1974; Fisk and Bence 1980). In samples from Jorullo and Cerro La Pilita, spinel cubes and clusters of cubes occur within olivine phenocrysts (Fig. 4) and locally in the groundmasses. Spinel may have been the liquidus phase acting as a nucleation site for olivine (Ridley 1977), but similar textural patterns have been interpreted as spinel nucleation upon olivine (Thy 1983). Thus the textural evidence is equivocal as to the first crystallizing phase. Liquidus $T-f_{O_2}$ estimates for Jor 44 (Table 9), however, are consistent with spinel as the liquidus mineral, probably closely followed by olivine.

Many previous studies of spinel compositional evolution have concerned reactions between spinel and olivine or melt during slow cooling of plutonic or holocrystalline volcanic rocks (Evans and Moore 1968; Ridley 1977; Lehmann 1983; Ozawa 1983). Spinels included in olivine phenocrysts of Jorullo lavas were rapidly quenched from near-liquidus conditions, and the compositional variations shown by these spinel-olivine pairs are interpreted as a sequence of quenched equilibrium states (Arculus 1974). As seen in Figs. 6 and 7, there is a nearly complete range of spinel compositions present from early magnesiochromites (Table 5 – #a), through chromites (#d), and titaniferous chromites (#g), to titanomagnetites (#h). This progressive sequence is marked by decreases in Mg, Al, and Cr, and increases in Ti, V, Fe^{+3}, Fe^{+2}, and Mn, similar to trends produced experimentally by decreasing T at constant f_{O_2} (Hill and Roeder 1974). Among the Jorullo spinels, Cr/(Cr+Al) remains relatively constant during early stages of evolution, then rapidly increases in the titaniferous chromites, and plummets to low values in the titanomagnetites (Fig. 6). The spinel Mg-number shows a smooth decrease through the series and correlates closely with the host olivine Mg-number as seen in Fig. 7.

Unlike the spinel Mg-number, the concentrations of Al^{+3}, Cr^{+3} and other important spinel constituents show

wide variations with respect to the host olivine Mg-number (Fig. 7). Thy (1983) observed similar large variations among included spinels and suggested that they reflect compositional gradients in the melt adjacent to growing olivine phenocrysts, upon which the spinel crystals nucleated heterogeneously. As discussed above, however, spinel probably preceded olivine in the Jorullo lavas, and therefore the compositional variations shown by the included spinels can only be explained by original compositional heterogeneities in the melt or variations in the characteristic diffusion volumes for competing spinel nuclei.

Spinels comprise an exceedingly complex mineral group in which numerous binary miscibility gaps have been recognized (Sack 1982). Haggerty (1972) demonstrated a complete range of compositions between chromite and ulvöspinel in lunar samples. Hill and Roeder (1974) produced a complete solid solution between chromite and titanomagnetite in basalt crystallization experiments at oxygen fugacities greater than 10^{-8} atm, but under more reducing conditions, chromite crystallization was interrupted by formation of clinopyroxene. Irvine (1967) discussed several possible reactions involved in terminating chromite crystallization in basaltic melts.

Among basaltic rocks, spinel compositional variations covering all or part of the chromite to titanomagnetite solid solution range have been described from ankaramites and oceanites of East Island, Indian Ocean (Gunn et al. 1970), a Snake River Plain basalt (Thompson 1973), basanitoids and alkali basalts from Grenada (Arculus 1974), Tertiary basalts from Rhum and Muck (Ridley 1977), sanukitoids from southwest Japan (Tatsumi and Ishizaka 1982a), and basanites and minettes from western Mexico (Luhr and Carmichael 1981), as well as the Jorullo and Cerro La Pilita samples. Complete solid solution is very difficult to demonstrate statistically since many intermediate compositions are only rarely represented. Sack (1982) discussed the strong temperature dependence of activity coefficients for $FM_2TiO_4-FMAl_2O_4$ spinel components during the transition to titanomagnetite. This transition may occur over a few tens of degrees, and in this manner, a continuous spinel solid solution series will be preserved in the rock as an essentially bimodal assemblage of chromite and titanomagnetite, with few intermediate compositions. As a further complication, many small groundmass spinels are strongly zoned from Cr-rich cores to titanomagnetite rims, and the activation volume of an electron probe beam is typically too large to discriminate continuous from discontinuous zoning (Gunn et al. 1970; Ridley 1977). As a result of these sampling and analytical uncertainties, it is unclear whether gaps in spinel compositional trends (Figs. 6 and 7) are real or artificial. The results of Hill and Roeder (1974) applied to the Jorullo suite, however, indicate that a complete solid solution from chromite to titanomagnetite should be present.

Origin of compositional variation among Jorullo lavas

Both the Parícutin and Jorullo eruptions produced progressively less-basic magmas with time, in sharp contrast to the usual course of silicic pyroclastic events, where eruption of progressively more-basic magmas is modeled as a simple inversion of a vertically stratified magma chamber (Hildreth 1981). Wilcox (1954) proposed a geometric explanation, whereby marginal tapping of a vertically stratified magma cupola caused it to drain progressively higher levels with time. Although such an explanation may also pertain in the Jorullo case, the similarity in unusual eruptive pattern at these two closely spaced volcanoes argues for a more fundamental cause.

The lavas of Jorullo range from early primitive basalts (Jor 44) to late basaltic andesites (Jor 7, 11, 28). The latter are similar in composition and mineralogy to the more-basic products erupted from many arc stratovolcanoes, which are often dominated by andesites (Wise 1969; Condie and Swenson 1973; Francis et al. 1974; Rose et al. 1977; Fairbrothers et al. 1978; Dixon and Batiza 1979; Newhall 1979; Luhr and Carmichael 1980; Gill 1981). The Jorullo basaltic andesites are also similar to the earliest, most-basic lavas of Parícutin. Thus, the Jorullo suite may serve as a model for the early stages of evolution in arc magmas, a compositional range that is rarely erupted in mature arcs and may never erupt from mature stratovolcanoes. Wilcox (1954) evaluated two classic mechanisms for the origin of compositional diversity among the Parícutin lavas: granitic assimilation and crystal fractionation. These same two end-member mechanisms are now independently evaluated for the Jorullo lavas, although it has long been recognized that assimilation cannot proceed without accompanying crystallization (Bowen 1928).

Assimilation

As discussed earlier, sharply-bounded granitic xenoliths are present in some Jorullo lavas, particularly those from the middle-stage satellite cones, and plagioclase xenocrysts can be found in almost any thin section. La Huacana Granite (LHG – Table 1) is taken as representative of the silicic plutonic end member prior to incorporation into the Jorullo magmas; three other analyses of basement granitic rocks are given in Appendix 2. Al, Ti, and Sr compositional trends in the Jorullo suite are incompatible with simple bulk assimilation of any of these silicic plutonic rocks; each of these elements increases with SiO_2 in the Jorullo suite, yet the silicic plutonic rocks have lower concentrations of these elements than any of the lavas. Other, less dramatic conflicts are shown by the data for Cu and Zn. Clearly, bulk granitic assimilation is incapable of explaining the compositional trends of the Jorullo lavas. Recent experiments by Watson (1982) and Watson and Jurewicz (1984) have demonstrated the high relative mobility of potassium and sodium during granite-basalt interaction, and preferential contamination by radiogenic Sr has been called upon to explain $^{87}Sr/^{86}Sr$ variations among cogenetic volcanic rocks of the high Andes (Briqueu and Lancelot 1979; Francis et al. 1980). Selective contamination of this type has not been evaluated in this study.

Crystal fractionation

Major-element least-squares crystal-fractionation models for deriving late-stage Jor 11 from early-stage Jor 44 were tested using the program XLFRAC (Stormer and Nicholls 1978). A small amount of Cr – Al – Mg spinel separation is necessary to reduce the concentration of Cr from 516 ppm (Jor 44) to 75 ppm (Jor 11), but spinel was not included in the major-element modeling. A variety of models were tested. Those involving only olivine, olivine + augite, or olivine + plagioclase gave very poor results ($\Sigma r^2 > 3$). Good results could only be obtained using all three minerals simultaneously ($\Sigma r^2 = 0.8$), and an excellent fit ($\Sigma r^2 = 0.07$)

Table 10. Crystal-fractionation model for the derivation of Jor 11 from Jor 44

	Jor 44	Jor 11 measured	Jor 11 predicted
SiO_2	52.61	54.80	54.92
TiO_2	0.82	0.93	0.97
Al_2O_3	16.60	18.96	19.01
FeO[t]	7.52	6.61	6.66
MnO	0.14	0.11	0.13
MgO	9.38	4.69	4.73
CaO	8.54	7.96	7.96
Na_2O	3.50	4.57	4.41
K_2O	0.75	1.12	1.01
P_2O_5	0.14	0.24	0.20
		$\Sigma r^2 = 0.07$	
Subtracted phases		wt% of initial magma	
olivine (Fo 90.5)		4.88	
olivine (Fo 73.3)		5.91	
plagioclase (An 76.1)		5.03	
augite ($Wo_{46}En_{44}Fs_{10}$)		7.29	
wt% crystallized		23.11	

was produced using augite, plagioclase, and two different olivine compositions ($Fo_{90.5}$: and $Fo_{73.3}$) to allow the program to calculate an average Fe/Mg ratio in olivine for the entire fractionation interval. The latter model is listed in Table 10. It calls for subtraction of 10.8% olivine (mean composition $Fo_{81.0}$), 7.3% augite, and 5.0% plagioclase ($An_{76.1}$) from Jor 44 to produce Jor 11. These relative abundances need not represent cotectic proportions in the fractionating basalt, since the minerals have different buoyancies in the melt. Grove and Baker (1984) recently stressed the importance of fractionation at moderate pressure of subequal proportions of olivine, augite, and plagioclase from parental basalt to produce derivative calc-alkaline magmas. Our model and theirs are in complete agreement on this point.

Using graphical constructions, Wilcox (1954) concluded that major-element variations in the Parícutin suite could be explained by combined crystal fractionation – granite assimilation, but not by crystal fractionation alone. In contrast, the major-element variations in the Jorullo suite can be satisfactorily explained by simple crystal fractionation. Other least-squares models were tested using LHG as an additional phase. Again, poor fits ($\Sigma r^2 > 2$) were obtained for all combinations of less than two minerals plus LHG. The model involving olivine + augite + plagioclase + LHG gives only a slightly better fit than the similar model without LHG (Table 10), but calls for subtraction of 1.4% LHG as well as the minerals. This model is physically unreasonable, and it is concluded that simple crystal fractionation is the process most consistent with major-element trends in the Jorullo lava suite. The inferred lack of significant granite assimilation at Jorullo is consistent with the sharp contacts of all granitic xenoliths in the middle-stage Jorullo lavas and the apparent lack of intimate blending between the lavas and inclusions. The xenoliths were probably picked up shortly before eruption as the Jorullo magmas passed through high-level granitic bodies. Wilcox (1954) also noted sharp basalt-granite xenolith contacts at Parícutin and a lack of "mixing and strewing of one material

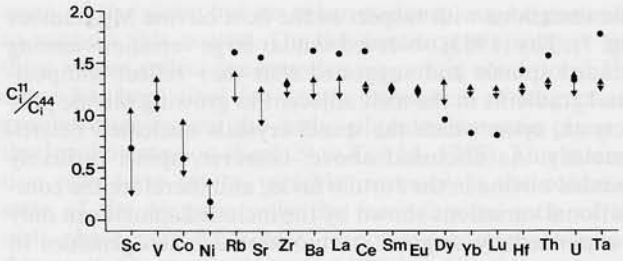

Fig. 9. Concentration ratios for 19 trace elements in Jor 11/Jor 44. Dots indicate measured ratios. Arrows indicate range of ratios for each trace element predicted by the least-squares major element model of Table 10 assuming Rayleigh fractionation (Arth 1976). Low values were computed using concentrations in Jor 44 minus analytical uncertainty and high partition coefficients from Table 11; high values were computed using concentrations in Jor 44 plus analytical uncertainty and low partition coefficients from Table 11

in the other". Nonetheless, he concluded that assimilation was a significant process at Parícutin, a conclusion that has been supported by recent isotopic studies (Reid 1983). The importance attributed to granitic assimilation is one of the major differences between the largely similar eruptions of Jorullo and Parícutin.

The concentrations of 19 trace elements in Jor 11 were predicted assuming Rayleigh fractionation of the mineral assemblage given by the major-element model (Table 10) and crystal-liquid partition coefficients for basalts taken from the literature (Table 11). Ranges of predicted concentrations for each element as ratios to the concentration in Jor 44 are shown by arrows on Fig. 9. These ranges reflect analytical uncertainties in the composition of parent Jor 44 and variations in published partition coefficients. Eight of the tested trace elements were successfully predicted by the fractionation model in that measured concentrations in Jor 11 (dots on Fig. 9) are bracketed by the calculated compositional range. These include the strongly compatible elements Sc, V, Co, and Ni, the middle REEs Sm and Eu, and the incompatible elements Zr and U.

Eleven elements were not successfully predicted. The three heavy REEs Dy, Yb, and Lu are anomalously depleted in Jor 11 compared to concentrations predicted by the major-element model (Fig. 9). As seen in Fig. 3, the chondrite-normalized REE patterns of Jor 44 and Jor 11 cross at Tb. The predicted pattern for Jor 11, however, is subparallel to that for Jor 44 (Fig. 3). The relative depletions of these heavy REEs in Jor 11 demand bulk distribution coefficients greater than unity. Although clinopyroxene preferentially accomodates heavy REEs, partition coefficients in Table 11 show maximum values of 1. Preferential depletion in heavy REEs may indicate crystallization of garnet, but no direct evidence exists to support this hypothesis. Therefore, depletion of the heavy REEs and the consequent crossing of chondrite-normalized patterns cannot be reconciled with simple crystal fractionation. The remaining eight elements are richer in Jor 11 than predicted by the major-element model. These include the incompatible elements Rb, Sr, Ba, La, Ce, Hf, Th, and Ta. Enrichment factors for these elements (= concentration in Jor 11/concentration in Jor 44) range from 1.42 (Hf) to 1.76 (Ta) as compared to a maximum possible enrichment factor (bulk distribution coefficient = 0) of 1.30 predicted from the major-element model. Similar excess enrichments of incompa-

Table 11. Partition coefficients used in crystal-fractionation model

	olivine	plagioclase	augite
Sc	0.15–0.4	0.01–0.07	2–20
V	0.04–0.05	0	0.2–1.6
Co	2–7	0.04–0.1	0.9–3
Ni	10–50	0.03–0.05	1–20
Rb	0.01–0.08	0.01–0.2	0.001–0.1
Sr	0.003–0.03	1–5	0.05–0.3
Zr	0.005–0.11	0.01–0.18	0.1–0.4
Ba	0.005–0.04	0.05–0.9	0.001–0.06
La	0.003–0.05	0.03–0.3	0.02–0.15
Ce	0.002–0.03	0.02–0.3	0.04–0.3
Sm	0.003–0.03	0.01–0.17	0.1–0.8
Eu	0.005–0.05	0.02–0.7	0.1–0.8
Dy	0.006–0.14	0.01–0.2	0.1–1.0
Yb	0.003–0.07	0.01–0.3	0.1–1.0
Lu	0.004–0.03	0.01–0.2	0.3–1.0
Hf	0.004–0.07	0.01–0.08	0.1–0.6
Th	0.01–0.05	0.01–0.07	0.001–0.07
U	0.01–0.07	0.01–0.08	0.001–0.07
Ta	0.01–0.05	0.02–0.06	0.05–0.07

Data from Higuchi and Nagasawa (1969), Schnetzler and Philpotts (1970), Nicholls and Harris (1980), Villemant et al. (1981), Dostal et al. (1983), Fujimaki et al. (1984), and compilations by Arth (1976) and Irving (1978)

tible elements have been observed for tholeiites from the Famous Area (Bryan et al. 1976; Bryan and Moore 1977; White and Bryan 1977; Bryan et al. 1979) and elsewhere in the Atlantic Ocean basin (Frey et al. 1974). A variety of hypotheses have been put forward to explain these anomalous enrichments, including: volatile fluxing of incompatible-element complexes toward magma-chamber margins (Bryan and Moore 1977), mixing of magmas derived from different degrees of partial melting (White and Bryan 1977), open magma chamber processes (Bryan et al. 1979; O'Hara 1977; O'Hara and Mathews 1981), and dynamic partial melting (Langmuir et al. 1977). The relatively low concentrations of MgO, Cr, and Ni in the late-stage Jorullo lavas indicate that these are not products of direct partial melting in the mantle. Thus partial-melting mechanisms are unsuitable for explaining excess enrichments in the Jorullo suite. The general success of the major-element model in Table 10 leads us to believe that the early- and late-stage Jorullo magmas are principally related through crystal fractionation, but that other processes were operating concurrently, leading to anomalous enrichments of light REEs and other incompatible trace elements, and anomalous depletions of heavy REEs. Selective elemental exchange with granitic wall rocks and xenoliths may have been important in this regard, but the process is not presently testable.

A common test of plausibility applied to least-squares-based fractionation models is to compare the predicted phase proportions to the observed mode of the parent rock. By this criterion, the model presented in Table 10 is a failure. High proportions of augite and plagioclase are calculated, yet neither mineral is present in the phenocryst population of Jor 44 (Table 4). Phenocryst-sized plagioclase crystals are present in middle-stage Jorullo lavas, but augite phenocrysts do not appear until the late-stage lavas. These observed trends are consistent with 1-atm crystallization experiments on Jor 44 (Mo and Carmichael, unpublished data), in which olivine appears on the liquidus at 1,260° C, plagioclase appears at 1,190° C, and augite was not present upon quenching at 1,160° C (Table 9).

Similar conflicts between modeled clinopyroxene fractionation and absence of clinopyroxene as a phenocryst phase have been commonly reported in studies of mid-ocean ridge tholeiites (Bryan et al. 1976; Bryan and Moore 1977; Dungan and Rhodes 1978; Rhodes et al. 1979; Shibata et al. 1979; Thompson et al. 1980; and Wilkinson 1982) as well as basalts from the Snake River Plain and Skye (Thompson 1972) and basalts from cinder cone fields behind the Central American Arc (Walker 1981). Numerous experimental studies on basaltic compositions have demonstrated that the clinopyroxene stability field increases with pressure, and that clinopyroxene eventually replaces olivine as the liquidus phase at pressures >9 kb (Green and Ringwood 1967; Bender et al. 1978; Stolper 1980; Baker and Eggler 1983). Accordingly, many of the above authors have explained the "clinopyroxene anomaly" by invoking relatively high-pressure fractionation involving clinopyroxene to generate the compositional diversity in a lava suite, followed by low-pressure, clinopyroxene-absent crystallization prior to eruption.

In Fig. 10, the Jorullo whole-rock analyses are plotted on three pseudoternary projections along with experimentally determined liquidus boundary curves taken from Walker et al. (1979), Stolper (1980), and Baker and Eggler (1983). We note that plots B and C (after Baker and Eggler 1983) account for ferric iron by projecting from magnetite, whereas plot A (after Walker et al. 1979) makes no provision for ferric iron. The Jorullo bulk compositions fall along moderate-pressure liquidus boundary curves involving olivine, augite, plagioclase, and liquid, and yet the early, most-basic lavas do not carry augite or plagioclase phenocrysts. Augite and plagioclase would both be near the liquidus at pressures from 8 to 15 kb, and therefore, the compositional diversity among the Jorullo lavas appears to have resulted primarily from crystal fractionation at lower-crustal to upper-mantle depths. Since the minerals actually present in the lavas are consistent with crystallization at low pressures, a two-stage crystallization history is implied. Similar conclusions were drawn by Baker and Eggler (1983) with regard to high-alumina basalts from Atka. Relict phenocrysts of augite and plagioclase from the earlier crystallization event may have been resorbed on route to the surface as their stability fields contracted, or as the magmas followed adiabatic gradients with shallower dT/dP slopes than the liquidus curves and approached a superheated condition.

Jor 44 and high-alumina basalts

General consensus has emerged among petrologists to favor an origin for most arc andesites through fractional crystallization of basalt (Bowen 1928; Green 1980; Perfit et al. 1980; Arculus 1981; Gill 1981; Anderson 1982; Carr et al. 1982; Dixon and Stern 1983; Sakuyama 1983; Grove and Baker 1984), with mixing of magmas and crustal assimilation playing minor modifying roles. Other andesites may be derived from primary high-Mg andesites (Kay 1978; Tatsumi and Ishizaka 1981, 1982a, 1982b), although there is little evidence to support such a mechanism in most cases. The nature of primitive arc basalt has been only poorly defined. By the criteria of Mg-number (63–73; Green 1971), FeO^T/MgO (<1; Tatsumi et al. 1983), and Ni content

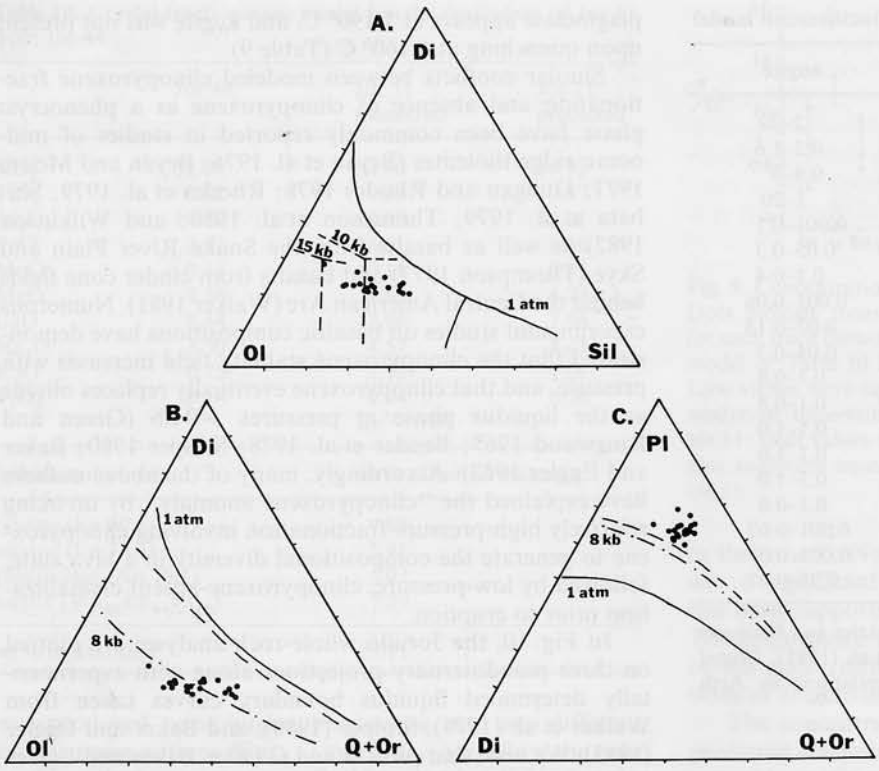

Fig. 10 A–C. Dots show whole-rock analyses of Jorullo lavas plotted on pseudoternary projections (mol%). **A** Plagioclase-saturated system Diopside – Olivine-Silica following Walker et al. (1979) with cotectics taken from Walker et al. (1979) and Stolper (1980). **B** Plagioclase-magnetite-saturated system Diopside – Olivine – Quartz + Orthoclase following Baker and Eggler (1983) with liquidus boundary curves at 1 atm (*solid*), 8 kb (*dash-dot*), and 0.5–2 kb with 2–3 wt% H_2O (*dashed*) taken from Baker and Eggler (1983). **C** Olivine-magnetite-saturated system Plagioclase – Diopside – Quartz + Orthoclase following Baker and Eggler (1983) with liquidus boundary curves as in B

(235–400 ppm; Sato 1977), few primitive arc basalts have been described. Kuno (1960) defined high-alumina basalt as a variety intermediate between tholeiitic and alkalic basalts, with greater than 16% Al_2O_3. Most workers accept high-alumina basalts as the parents of arc andesites, but the majority of high-alumina basalts described in the literature, though very high in Al_2O_3 (18–21 wt%), are too depleted in MgO, Ni, and Cr to qualify as primitive mantle-derived magmas (see analyses in Lopez-Escobar et al. 1977, 1981; Carr et al. 1982; Marsh 1982). As noted by Perfit et al. (1980), Uto (1981), and Kay et al. (1982), Al_2O_3 in arc basalts generally increases with differentiation (FeO^t/MgO). This has been taken to indicate a plagioclase-absent fractionation mechanism. A similar trend is shown by the Jorullo lavas, however, and the least-squares model of Table 10 demonstrates that this trend is consistent with fractionation of an assemblage containing 22% plagioclase. Fig. 11 is a plot of whole-rock concentrations of MgO vs. Al_2O_3. The Jorullo samples, represented by solid symbols, show a negative linear correlation between these elements. Kuno's type-specimen high-alumina basalts are indicated by open squares and other high-alumina basalts are shown by open circles (Lopez-Escobar et al. 1977) and open triangles (Ewart 1976). All of these high-alumina basalts fall near the low-MgO, high-Al_2O_3, differentiated end of the Jorullo trend. We conclude that most high-alumina basalts described in the literature have suffered significant fractionation from a primitive, parental basalt (Lopez-Escobar et al. 1977 and 1981; Nicholls 1978; Perfit et al. 1980). Crystallization of olivine and spinel are particularly important in reducing the Cr and Ni contents and Mg-numbers of these derivative basalts. The high Al_2O_3 contents can themselves be taken as evidence of a protracted crystallization history prior to eruption (Green and Ringwood 1967; Lewis 1971; Holloway and Burnham 1972). The Jorullo lava suite may serve as a model for the earliest stages of

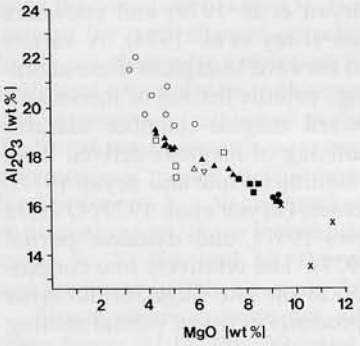

Fig. 11. MgO vs. Al_2O_3 variation diagram for whole-rock samples. Solid symbols represent the Jorullo lavas: *circles* = early-stage, *squares* = middle-stage, *triangles* = late-stage. Open squares are the type specimen high-alumina basalts of Kuno (1960). Open circles are high-alumina basalts from Lopez-Escobar et al. (1977). Open triangles basalts from Ewart (1976): upright triangle – average of western American basalts, inverted triangle – average of island arc basalts. Crosses represent three basaltic sanukitoids from Japan (Tatsumi and Ishizaka 1982a: samples 438 and 424; and 1982b: sample SG-1)

fractionation from calc-alkaline basalt. As discussed earlier, fractionation of Jorullo basalts to basaltic andesites probably occurred in the lower crust or upper mantle. Basaltic andesite, similar to the late-stage Jorullo lavas, may be the most common magma type rising from depth in arc terrains and feeding shallow-level magma chambers wherein andesites, dacites, and rhyodacites are produced through low-pressure crystallization.

Early-stage Jorullo lavas are characteristically rich in SiO_2; Jor 44, which qualifies as a primitive basalt, has over 52 wt% SiO_2. These relatively high SiO_2 contents may reflect relatively hydrous conditions in the mantle during partial melting (Kushiro 1972). We also note a strong composi-

tional similarity between the early Jorullo basalts and basaltic sanukitoids from the Setouchi volcanic belt of southwest Japan (Tatsumi and Ishizaka 1982a and 1982b). Three of these basaltic sanukitoids are plotted on Fig. 11 as crosses. One of them (SG-1) is virtually indistinguishable in bulk composition from Jor 44. Tatsumi (1982) has demonstrated that silica-rich primitive sanukitoids can coexist with a lherzolite mineral assemblage under both water-saturated and -undersaturated conditions.

Trachybasalts from Cerro La Pilita

Systematic compositional variations with distance from the trench have long been recognized in the Japanese and other subduction-related arcs (Rittman 1953; Kuno 1959; Sugimura 1960, 1968; Dickinson and Hatherton 1967; Gill 1981). In these arcs, erupted magmas generally become more alkalic and undersaturated in silica away from the trench. As other arcs have been studied in greater detail, however, exceptions to these systematic compositional progressions have been documented (Arculus and Johnson 1978). We previously detailed the simultaneous eruptions of calc-alkaline and highly alkaline magmas in the southern Colima graben of western Mexico, some 200 km west of Jorullo (Luhr and Carmichael 1980, 1981, 1982). Within the Michoacán-Guanajuato Volcanic Field, Hasenaka and Carmichael (1985) have identified statistically significant compositional trends with increasing distance from the Middle America Trench; magmas of similar silica content become increasingly enriched in K_2O and incompatible elements landward, as concentrations of MgO, Cr, and Ni fall. The near-trench Jorullo lavas, high in MgO, Cr, and Ni, conform to this general pattern. A small number of eruptive centers in the volcanic field, however, deviate markedly in mineralogy and composition from the general patterns. One of the most dramatic deviations is shown by Cerro La Pilita, the late-Quaternary cinder cone with associated lava flow that sits just 3 km south of the main cone of Jorullo. Cerro La Pilita produced ne-normative trachybasalts, with high concentrations of MgO, Cr, Co, and Ni, similar to those in the early Jorullo basalts, but containing much higher concentrations of K_2O, P_2O_5, Sr, Zr, Ba, LREE's, Hf, Th, U, and Ta (Tables 1, 2, and 3). The trachybasalts also differ from the Jorullo basalts mineralogically, containing spinel richer in Fe^{+3}, phenocrysts and microphenocrysts of relatively potassic hornblende, and microphenocrysts of apatite, in addition to olivine, augite, and plagioclase. The Cerro La Pilita trachybasalts record significantly higher water contents and oxygen fugacities compared to the early-stage Jorullo basalts, as reflected in the presence of hornblende and Fe^{+3}-rich spinel and in higher whole-rock $Fe^{+3}/Fe^{+3}+Fe^{+2}$.

Both the early basalts of Jorullo and the trachybasalts of Cerro La Pilita qualify as primitive magmas. There are differences up to ten-fold in their concentrations of many incompatible elements, and no likely crystal fractionation or bulk crustal assimilation scheme can relate the two magmas; they probably represent fundamentally different partial melting events in the underlying mantle. Based on the experiments of Kushiro (1968), the ne-normative trachybasalts were probably generated at considerably higher pressure. In the case of the southern Colima graben, we similarly found no evidence for a simple relationship between the two magma suites (Luhr and Carmichael 1981). There, the major graben structure may be intimately related to the eruption of highly alkaline magmas, but no evidence of extensional tectonism exists in the Jorullo area. These incompatible-element-enriched, silica-undersaturated magmas erupting along the volcanic front in Mexico, are rare but highly significant deviations from the dominant spatial-compositional trends, and their origin constitutes one of the greatest outstanding problems in modeling the development of this exceedingly complex continental arc.

Conclusions

It is difficult to avoid comparisons between Jorullo (1759–1774) and Parícutin (1943–1952), the only two historically active volcanoes in one of the largest cinder cone fields on earth. Both eruptions produced: 1) a new volcano: Jorullo rising from a ravine and Parícutin from a corn field; 2) 1–2 km^3 of magma progressing to compositions richer in SiO_2 with time; and 3) lavas containing angular xenoliths of basement granites. The products of Parícutin ranged from early basaltic andesites to late andesites, a compositional trend which is consistent with derivation by combined crystal fractionation – assimilation (Wilcox 1954; Reid 1983). The products of Jorullo, in contrast, ranged from early primitive basalts to late basaltic andesites, a compositional trend most consistent with simple crystal fractionation of olivine + augite + plagioclase + minor spinel at lower-crustal to upper-mantle pressures. Early-formed augite and plagioclase phenocrysts were effectively removed from the Jorullo lavas prior to eruption; the actual minerals in the lavas appear to have crystallized at low pressure. The light REEs (La, Ce) and other incompatible trace elements (Rb, Sr, Ba, Hf, Th, Ta) are anomalously enriched in the late-stage lavas, whereas the heavy REEs (Dy, Yb, Lu) are anomalously depleted. These trends, which result in crossed chondrite-normalized REE patterns, apparently indicate the operation of other magma chamber processes accompanying crystal fractionation.

With increasing fractionation in the Jorullo suite, there are decreases in whole-rock concentrations of MgO, Cr, Co, and Ni, and increases in SiO_2, Al_2O_3, and incompatible elements. Many of the most-basic lavas erupted in subduction-related arcs are basalts with high Al_2O_3, but low MgO, Cr, Co, and Ni. These basalts have probably undergone considerable fractionation from a primitive parental magma similar to the early Jorullo basalts.

Cerro La Pilita, a late-Quaternary cinder cone centered just 3 km south of Jorullo, produced a fundamentally different suite of primitive, silica-undersaturated trachybasalts, far richer than the Jorullo basalts in K_2O, P_2O_5, Sr, Ba, and many other incompatible elements, and containing hornblende and apatite crystals. Such strong contrasts in closely erupted magma suites negate simple petrogenetic models for the Mexican Volcanic Belt.

Acknowledgments. Jamie Allan, Toshi Hasenaka, Mike Kokinos, Mike Kosca, Xuan-Xue Mo, and Neil Summer assisted us in our field studies at Jorullo. Joachim Hampel performed alkali analyses by flame photometer and photographed the diagrams. INA data were obtained through Helen Michel and Frank Asaro. S.A. Morse and A. Ewart provided careful reviews of the manuscript. We express our appreciation to all of these individuals. We are also grateful to the residents of La Puerta de la Playa for their kindness and hospitality during our visits to Jorullo. This research was supported by NSF grants EAR 80-06043 and EAR 81-03344 to Carmichael.

Appendix 1. Additional whole-rock analyses by XRF of Jorullo lavas

Jor	19	25	39B	29	42	26	27	15	2	16	35	5	6	10
Group	E	E	M	M	M	L	L	L	L	L	L	L	L	L
Lat (18°)	58.60′	58.30′	57.79′	59.09′	58.09′	58.84′	58.93′	58.46′	58.95′	58.42′	59.21′	58.63′	58.57′	58.66′
Long (101°)	45.20′	44.90′	43.88′	42.92′	44.28′	43.92′	43.91′	42.55′	44.22′	42.55′	43.30′	43.07′	43.10′	43.29′
SiO_2	52.62	52.96	53.18	53.32	53.28	53.97	54.72	53.82	54.00	53.27	54.41	55.08	54.78	54.86
TiO_2	0.82	0.83	0.79	0.89	0.81	1.00	0.99	0.99	0.99	0.99	0.98	0.97	0.96	0.96
Al_2O_3	16.35	16.14	16.13	16.82	16.55	17.83	18.37	17.49	17.60	17.23	18.31	18.42	18.93	18.51
Fe_2O_3	1.78	1.63	2.48	2.22	2.71	1.52	1.74	1.83	1.43	1.68	1.77	2.22	2.37	2.44
FeO	5.76	5.98	5.02	5.26	4.62	5.48	5.07	5.44	5.71	5.69	4.96	4.40	4.32	4.41
MnO	0.13	0.13	0.13	0.13	0.12	0.12	0.12	0.12	0.12	0.12	0.11	0.11	0.11	0.11
MgO	9.05	9.37	9.20	8.17	8.25	6.20	5.13	7.27	6.67	7.45	4.95	4.65	4.36	4.72
CaO	8.60	8.42	8.38	8.33	8.27	8.18	8.14	8.13	8.09	8.08	8.03	7.93	7.84	7.78
Na_2O	3.76	3.57	3.61	3.67	3.62	4.10	4.20	3.84	4.01	3.83	4.36	4.41	4.36	4.36
K_2O	0.78	0.75	0.79	0.82	0.86	0.97	1.01	0.91	0.95	0.90	1.03	1.05	1.09	1.07
P_2O_5	0.15	0.15	0.16	0.17	0.17	0.21	0.22	0.21	0.20	0.20	0.22	0.22	0.23	0.23
LOI	0.75	0.59	0.75	0.73	0.61	0.68	0.65	0.57	0.71	0.05	0.68	0.61	0.59	0.58
Total	100.55	100.52	100.62	100.53	99.87	100.26	100.36	100.62	100.48	99.49	99.81	100.07	99.94	100.03
Trace elements (ppm)														
V	202	202	210	202	227	191	172	216	202	240	191	194	200	191
Cr	523	563	555	411	462	215	137	275	297	326	153	86	47	73
Ni	223	265	241	194	183	93	50	132	108	148	37	38	28	47
Cu	53	55	52	56	64	41	48	48	47	45	38	42	41	38
Zn	59	66	65	71	64	66	71	61	69	72	65	59	71	75
Ga	17	17	20	18	15	22	20	19	18	20	15	22	21	22
Rb	12	12	13	14	20	14	16	15	14	17	14	15	16	18
Sr	394	402	423	451	439	526	560	502	518	500	573	597	628	605
Y	21	24	16	17	16	19	18	17	18	15	19	18	22	20
Zr	106	108	100	114	109	125	134	128	118	128	128	133	132	127
Nb	12	12	14	13	12	14	9	12	15	15	13	12	13	12
Ba	216	200	240	248	246	280	291	263	276	256	295	315	327	320
La	5	12	11	8	7	10	17	14	12	9	15	9	13	11
Ce	18	18	13	18	19	35	21	22	28	22	29	26	25	26

Major elements determined on glasses fused with Li-tetraborate at F⋕M
Trace elements determined on pressed-powder pellets at UCB

Appendix 2. Whole-rock analyses by XRF of older lava and basement samples

Jor	45	9	23	24	38	21
P.T.	BA	B	G	G	G	G
Lat (18°)	60.59′	58.64′	58.35′	58.09′	57.52′	58.26′
Long (101°)	45.19′	43.81′	45.03′	44.95′	43.77′	45.28′
SiO_2	56.32	52.24	63.54	64.84	65.37	75.99
TiO_2	0.75	1.04	0.96	0.74	0.76	0.24
Al_2O_3	17.58	17.51	15.45	15.47	14.57	12.17
Fe_2O_3	2.21	6.37	5.75	1.80	1.90	0.82
FeO	4.02	2.72	0.40	3.05	3.06	0.10
MnO	0.10	0.15	0.03	0.07	0.08	0.04
MgO	5.99	5.22	3.19	2.45	2.27	0.05
CaO	7.21	8.22	4.82	4.16	3.97	0.46
Na_2O	4.10	4.05	3.62	3.53	3.32	2.73
K_2O	1.00	1.19	0.21	3.46	3.95	5.95
P_2O_5	0.10	0.19	0.18	0.17	0.13	0.03
LOI	0.46	1.52	2.86	0.73	0.58	0.55
Total	99.93	100.42	101.01	100.47	99.96	99.13

P.T. = petrographic type (B = basalt, BA = basaltic andesite, G = granite)
45 – old lava flow north of Playa de Guadalupe
9 – altered basalt from Cerro Partido

Appendix 2. (continued)

Jor	45	9	23	24	38	21
P.T.	BA	B	G	G	G	G
Lat (18°)	60.59′	58.64′	58.35′	58.09′	57.52′	58.26′
Long (101°)	45.19′	43.81′	45.03′	44.95′	43.77′	45.28′
Trace elements (ppm)						
Cr	356	–	12	–	14	44
Ni	161	18	26	4	16	21
Cu	44	13	15	62	176	52
Zn	78	69	31	32	51	54
Ga	20	20	16	11	16	15
Rb	13	38	15	406	158	158
Sr	554	379	233	54	154	218
Y	13	23	39	47	28	26
Zr	97	87	307	119	273	225
Nb	5	6	7	9	10	8
Ba	380	260	101	352	572	574
La	14	12	37	45	16	20
Ce	30	29	86	82	45	51

23 – small basement hill east of Agua Blanca
24 – small basement hill east of Agua Blanca
38 – southeast flank of Cerro Las Cuevas
21 – small basement hill east of Agua Blanca

References

Allen JC, Boettcher AL, Marland G (1975) Amphiboles in andesite and basalt: I. Stability as a function of $P-T-f_{O_2}$. Am Mineral 60:1069–1085

Allen JC, Boettcher AL (1978) Amphiboles in andesite and basalt: II. Stability as a function of $P-T-f_{H_2O}-f_{O_2}$. Am Mineral 63:1074–1087

Allen JC, Boettcher AL (1983) The stability of amphibole in andesite and basalt at high pressures. Am Mineral 68:307–314

Anderson AT Jr (1982) Parental basalts in subduction zones: Implications for continental evolution. J Geophys Res 87, B8:7047–7060

Arculus RJ (1974) Solid solution characteristics of spinels: Pleonaste-chromite-magnetite compositions in some island-arc basalts. Ann Rep Director Geophys Lab Yearb 73:322–327

Arculus RJ (1981) Island arc magmatism in relation to the evolution of the crust and mantle, Tectonophysics 75:113–133

Arculus RJ, Johnson RW (1978) Criticism of generalized models for the magmatic evolution of arc-trench systems. Earth Planet Sci Lett 39:118–126

Arth JG (1976) Behavior of trace elements during magmatic processes – A summary of theoretical models and their applications. USGS J Res 4, 1:41–47

Baker DR, Eggler DH (1983) Fractionation paths of Atka (Aleutians) high-alumina basalts: Constraints from phase relations. J Volc Geoth Res 18:387–404

Bender JF, Hodges FN, Bence AE (1978) Petrogenesis of basalts from the Project Famous area: Experimental study from 0 to 15 kbars. Earth Planet Sci Lett 41:277–302

Bowen NL (1928) The evolution of the igneous rocks. University Press, Princeton

Briqueu L, Lancelot JR (1979) Rb-Sr systematics and crustal contamination models for calc-alkaline igneous rocks. Earth Planet Sci Lett 43:385–396

Bryan WB, Moore JG (1977) Compositional variations of young basalts in the Mid-Atlantic Ridge rift valley near lat. 36°49′ N. Geol Soc Am Bull 88:556–570

Bryan WB, Thompson G, Frey FA, Dickey JS (1976) Inferred settings and differentiation in basalts from the Deep-Sea Drilling Project. J Geophys Res 81:4285–4304

Bryan WB, Thompson G, Michael PJ (1979) Compositional variation in a steady-state magma chamber: Mid-Atlantic Ridge at 36°50′ N. Tectonophysics 55:63–85

Bullard FM (1976) Volcanoes of the Earth. Univ Texas Press, Austin, p 579

Carmichael ISE (1967) The iron-titanium oxides of salic volcanic rocks and their associated ferromagnesian silicates. Contrib Mineral Petrol 14:36–64

Carr MJ, Rose WI, Stoiber RE (1982) Central America. In: Thorpe RS (ed) Orogenic Andesites and Related Rocks. Wiley, New York, pp 149–166

Clark KF, Foster CT, Damon PE (1982) Cenozoic mineral deposits and subduction-related magmatic arcs in Mexico. Geol Soc Am Bull 93:533–544

Condie KC, Swenson DH (1973) Compositional variations in three Cascade stratovolcanoes: Jefferson, Ranier, and Shasta. Bull Volcanol 37:205–230

Demant A (1981) L'axe neo-volcanique transmexicain: Estude volcanologique et petrographique signification geodynamique. Unpubl DSc dissert, Univ D'aix-Marseille, p 259

Dickinson WR, Hatherton T (1967) Andesitic volcanism and seismicity around the Pacific. Science 157, 3790:801–803

Dixon TH, Batiza R (1979) Petrology and chemistry of recent lavas in the Northern Marianas: Implications for the origin of island arc basalts. Contrib Mineral Petrol 70:167–181

Dixon TH, Stern RJ (1983) Petrology, chemistry, and isotopic composition of submarine volcanoes in the southern Mariana arc. Geol Soc Am Bull 94:1159–1172

Dostal J, Dupuy C, Carron JP, Le Guen de Kerneizon M, Maury RC (1983) Partition coefficients of trace elements: application to volcanic rocks of St. Vincent, West Indies. Geochim Cosmoch Acta 47:525–533

Dungan MA, Rhodes JM (1978) Residual glasses and melt inclusions in basalts from DSDP Legs 45 and 46: Evidence for magma mixing. Contrib Mineral Petrol 67:417–431

Eggler DH (1972) Water-saturated and undersaturated melting relations in a Paricutin andesite and an estimate of water content in the natural magma. Contrib Mineral Petrol 34:261–271

Eggler DH, Burnham CW (1973) Crystallization and fractionation trends in the system andesite-H_2O-CO_2-O_2 at pressures to 10 Kb. Geol Soc. Am Bull 84:2517–2532

Eugster HP, Wones DR (1962) Stability relations of the ferruginous biotite, annite. J Petrol 3:82–125

Evans BW, Moore JG (1968) Mineralogy as a function of depth in the prehistoric Makaopuhi tholeiitic lava lake, Hawaii. Contrib Mineral Petrol 17:85–115

Ewart A (1976) Mineralogy and chemistry of modern orogenic lavas – some statistics and implications. Earth Planet Sci Lett 31:417–432

Fairbrothers GE, Carr MJ, Mayfield DG (1978) Temporal magmatic variation at Boqueron Volcano, El Salvador. Contrib Mineral Petrol 67:1–9

Fisher RV, Heiken G (1982) Mt. Pelee, Martinique: May 8 and 20, 1902, pyroclastic flows and surges. J Volcanol Geotherm Res 13:339–371

Fisk MR, Bence AE (1980) Experimental crystallization of chrome spinel in Famous basalt 527-1-1. Earth Planet Sci Lett 48:111–123

Foshag WF, Gonzalez JR (1954) Birth and development of Parícutin Volcano, Mexico. USGS Bull 965-D:355–489

Francis PW, Roobol MJ, Walker GPL, Cobbold PR, Coward M (1974) The San Pedro and San Pablo volcanoes of northern Chile and their hot avalanche deposits. Geol Rundsch 63:357–388

Francis PW, Thorpe RS, Moorbath S, Kretzschmar GA, Hammill M (1980) Strontium isotope evidence for crustal contamination of calc-alkaline volcanic rocks from Cerro Galan, Northwest Argentina. Earth Planet Sci Lett 48:257–267

Frey FA, Bryan WB, Thompson G (1974) Atlantic Ocean floor: Geochemistry and petrology of basalts from Legs 2 and 3 of the Deep-Sea Drilling Project. J Geophys Res 79, 35:5507–5527

Fries C Jr (1953) Volumes and weights of pyroclastic material, lava, and water erupted by Parícutin Volcano, Michoacán, Mexico. Trans Am Geophy Un 34, 4:603–616

Fujimaki H, Tatsumoto M, Aoki K (1984) Partition coefficients of Hf, Zr, and REE between phenocrysts and groundmasses. J Geophys Res 89:B662–B672

Gadow H (1930) Jorullo: The history of the volcano of Jorullo and the reclamation of the devastated district by animals and plants. Cambridge Univ Press, London, p 101

Gill JB (1981) Orogenic andesites and plate tectonics. Springer, Berlin, p 391

Green DH (1971) Composition of basaltic magmas as indicators of conditions of origin: Application to oceanic volcanism. Phil Trans Roy Soc Lond A268:707–725

Green TH (1980) Island arc and continent-building magmatism – A review of petrogenetic models based on experimental petrology and geochemistry. Tectonophysics 63:367–385

Greene MT (1982) Geology in the nineteenth century – changing views of a changing world. Cornell Univ Press, Ithaca:324

Green DH, Ringwood AE (1967) The genesis of basaltic magmas. Contrib Mineral Petrol 15:103–190

Grove TL, Baker MB (1984) Phase equilibrium controls on the tholeiitic versus calc-alkaline differentiation trends. J Geophys Res 89, B5:3253–3274

Gunn BM, Coy-Yll R, Watkins ND, Abranson CE, Nougier J (1970) Geochemistry of an oceanite-ankaramite-basalt suite from East Island, Crozet Archipelago. Contrib Mineral Petrol 28:319–339

Haggerty SE (1972) Solid solution characteristics of lunar spinels. Ann Rep Director Geophys Lab Yearb 71:474–480

Hasenaka T, Carmichael ISE (1985) The Michoacán-Guanajuato Volcanic Field, central Mexico. Estimation of eruption age and volume of cinder cones. J Volcanol Geotherm Res (in press)

Higuchi H, Nagasawa (1969) Partition of trace elements between rock-forming minerals and the host volcanic rocks. Earth Planet Sci Lett 7:281–287

Hildreth W (1981) Gradients in silicic magma chambers: Implications for lithospheric magmatism. J Geophys Res 86, B11:10153–10192

Hill R, Roeder P (1974) The crystallization of spinel from basaltic liquid as a function of oxygen fugacity. J Geology 82:709–729

Holloway JR, Burnham CW (1972) Melting relations of basalt with equilibrium water pressure less than total pressure. J Petrol 13:1–29

Huebner JS (1969) Stability relations of rhodochrosite in the system manganese – carbon – oxygen. Am Mineral 54:457–481

Irvine TN (1967) Chromian spinel as a petrogenetic indicator: Part 2. Petrologic applications. Can J Earth Sci 4:71–103

Irving AJ (1978) A review of experimental studies of crystal/liquid trace element partitioning. Geochim Cosmoch Acta 42:743–770

Kay RW (1978) Aleutian magnesian andesites – Melts from subducted Pacific Ocean crust. J Volcanol Geotherm Res 4:117–132

Kay SM, Kay RW, Citron GP (1982) Tectonic controls on tholeiitic and calc-alkaline magmatism in the Aleutian arc. J Geophys Res 87, B5:4051–4072

Kuno H (1950) Petrology of Hakone Volcano and the adjacent areas, Japan. Geol Soc Am Bull 61:957–1020

Kuno H (1959) Origin of cenozoic petrographic provinces of Japan and surrounding areas. Bull Volc 20:37–76

Kuno H (1960) High-alumina basalt. J Petrol 1, 2:121–145

Kushiro I (1968) Compositions of magmas formed by partial zone melting of the earth's upper mantle. J Geophys Res 73:619–634

Kushiro I (1972) Effect of water on the compositions of magmas formed at high pressures. J Petrol 13:311–334

Langmuir CH, Bender JF, Bence AE, Hanson GN (1977) Petrogenesis of basalts from the Famous Area: Mid-Atlantic Ridge. Earth Planet Sci Lett 36:133–156

Lehmann J (1983) Diffusion between olivine and spinel: application to geothermometry. Earth Planet Sci Lett 64:123–138

Lewis JF (1971) Composition, origin, and differentiation of basalt magma in the Lesser Antilles. In: T.W. Donnelly (ed), Caribbean, geophysical, tectonic, and petrologic studies. Geol Soc Am Mem 130:159–179

Lofgren GE, Donaldson CH, Williams RJ, Mullins O, Usselman TM (1974) Experimentally reproduced textures and mineral chemistry of Appolo 15 quartz normative basalts. Proc Lunar Sci Conf 5:549–568

Lopez-Escobar L, Frey FA, Vergara M (1977) Andesites and high-alumina basalts from the central-south Chile High Andes: Geochemical evidence bearing on their petrogenesis. Contrib Mineral Petrol 63:199–228

Lopez-Escobar L, Vergara M, Frey FA (1981) Petrology and geochemistry of lavas from Antuco Volcano, a basaltic volcano of the southern Andes (37°25′ S). J Volcanol Geotherm Res 11:329–352

Luhr JF, Carmichael ISE (1980) The Colima Volcanic Complex, Mexico: I. Post-caldera andesites from Volcán Colima. Contrib Mineral Petrol 71:343–372

Luhr JF, Carmichael ISE (1981) The Colima Volcanic Complex, Mexico: II. Late-Quaternary cinder cones. Contrib Mineral Petrol 76:127–147

Luhr JF, Carmichael ISE (1982) The Colima Volcanic Complex, Mexico: III. Ash- and scoria-fall deposits from the upper slopes of Volcán Colima. Contrib Mineral Petrol 80:262–275

Marsh BD (1982) The Aleutians. In: R.S. Thorpe (Ed) Orogenic andesites and related rocks. Wiley, New York, pp 99–113

Masuda A, Nakamura N, Tanaka T (1973) Fine structures of mutually normalized rare-earth patterns of chondrites. Geochim Cosmochim Acta 37:239–248

Minster JB, Jordan TH (1978) Present-day plate motions. J Geophys Res 83:5331–5334

Molnar P, Sykes LR (1969) Tectonics of the Caribbean and Middle America regions from focal mechanisms and seismicity. Geol Soc Am Bull 80:1639–1684

Mooser F (1958) Active volcanoes of Mexico. Int Volc Assn Catelogue Active Volcanoes Part VI:36

Nakamura K (1977) Volcanoes as possible indicators of tectonic stress orientation – principal and proposal. J Volcanol Geotherm Res 2:1–16

Newhall CG (1979) Temporal variation in the lavas of Mayon Volcano, Philippines, J Volcanol Geotherm Res 6:61–83

Nicholls IA (1978) Primary basaltic magmas for the pre-caldera volcanic rocks of Santorini. Thera and the Aegean World I:109–120

Nicholls IA, Harris KL (1980) Experimental rare earth element partition coefficients for garnet, clinopyroxene and amphibole coexisting with andesitic and basaltic liquids. Geochim Cosmoch Acta 44:287–308

Nixon GT (1982) The relationship between Quaternary volcanism in central Mexico and the seismicity and structure of subducted ocean lithosphere. Geol Soc Am Bull 93:514–523

O'Hara MJ (1977) Geochemical evolution during fractional crystallisation of a periodically refilled magma chamber. Nature 266:503–507

O'Hara MJ, Mathews RE (1981) Geochemical evolution in an advancing, periodically replenished, periodically tapped, continuously fractionated magma chamber. J Geol Soc Lond 138:237–277

Ozawa K (1983) Evaluation of olivine-spinel geothermometry as an indicator of thermal history for peridotites. Contrib Mineral Petrol 82:52–65

Perfit MR, Gust DA, Bence AE, Arculus RJ, Taylor SR (1980) Chemical characteristics of island-arc basalts: Implications for mantle sources. Chem Geol 30:227–256

Perlman I, Asaro F (1969) Pottery analysis by neutron activation. Archaeometry 11:21–52

Reid MR (1983) Parícutin Volcano revisited: Isotopic and trace element evidence for crustal assimilation. Am Geophys Un Trans 64, 45:907

Rhodes JM, Dungan MA, Blanchard DP, Long PE (1979) Magma mixing at mid-ocean ridges: Evidence from basalts drilled near 22° N on the Mid-Atlantic Ridge. Tectonophysics 55:35–61

Ridley WI (1977) The crystallization trends of spinels in Tertiary basalts from Rhum and Muck and their petrogenetic significance. Contrib Mineral Petrol 64:243–255

Rittman A (1953) Magmatic character and tectonic position of the Indonesian volcanoes. Bull Volc 14:45

Roeder PL, Emslie RF (1970) Olivine-liquid equilibrium. Contrib Mineral Petrol 29:275–289

Robool MJ, Smith AL (1975) A comparison of the Recent eruptions of Mt Pelee, Martinique and Soufriere, St. Vincent. Bull Volc 39–2:1–27

Rose WI Jr, Grant NK, Hahn GA, Lange IM, Powell JL, Easter J, DeGraff JM (1977) The evolution of Santa Maria Volcano, Guatemala. J Geol 85:63–87

Sack RO (1982) Spinels as petrogenetic indicators: Activity-composition relations at low pressures. Contrib Mineral Petrol 79:169–186

Sack RO, Carmichael ISE, Rivers M, Ghiorso MS (1980) Ferric-ferrous equilibria in natural silicate liquids at 1 bar. Contrib Mineral Petrol 75:369–376

Sakuyama M (1983) Petrology of arc volcanic rocks and their origin by mantle diapirs. J Volcanol Geoth Res 18:297–320

Sato H (1977) Nickel content of basaltic magmas: Identification of primary magma and a measure of the degree of olivine fractionation. Lithos 10:113–120

Schnetzler CC, Philpotts JA (1970) Partition coefficients of rare-earth elements between igneous matrix material and rock-forming mineral phenocrysts – II. Geochim Cosmoch Acta 34:331–340